UNIVERSITAT POLITÈCNICA DE CATALUNYA
BARCELONATECH
Escola Superior d'Enginyeries Industrial,
Aeroespacial i Audiovisual de Terrassa

Study of the control for the recovery of a rocket's launch system

Document:
Report

Author:
Angel Pan Du

Director:
Fatiha Nejjari Akhi-Elarab

Degree:
Bachelor's degree in Aerospace Technology Enginneering

Examination session:
Spring, 2021

BACHELOR FINAL THESIS

Abstract

The research of advanced and innovative technologies is one of the main concerns within the aerospace industry. Spacecraft reusability is one of them, being an important aspect to diminish the huge costs and resources that a space mission implicate, minimising also the environmental impact.

This thesis develops the study and the implementation of the control for the safe recovery of the launch system of a rocket.

In order to accomplish this analysis, the current successful reusable rockets are evaluated and the Falcon 9 from the SpaceX is selected as the main model in which the project is focused on. Once characterised this particular system, the problem equation modelling is determined to create a framework within a Matlab environment and perform simulations.

The need of a control system is inferred through the first simulations results due to the lack of the safe landing parameters, being the most important a final velocity close to 0. Consequently, different linear controllers are proposed and compared to achieve the desired behaviour from the system. Nevertheless, the non-linearity of the problem added to these controllers limitations increase the complexity, due to the considerable quantity of control inputs. For these reasons, the system is simplified by computing the resultant forces and moments that the overall control surfaces must contribute. Following this methodology, the developed system consists in controlling the velocity with the forces and the pitch angle with the moments. From this last, the extracted conclusion is the Model Predictive Control tendency to dispose of a better adjustment to the setpoint rather than the PID.

In definitive, the limitations of these controllers have an impact to the final response and, for this reason, more complex proposals would be required to acquire an even closer approach to the real problem, such as nonlinear controllers or a second level of these type of controllers to determine the performance of each control device from the resultants of the forces and the moments, which are the inputs of the already controlled system.

Resum

La investigació sobre l'avenç i la innovació tecnològica és un dels principals objectes d'estudi en la indústria aeroespacial. El reús de vehicles espacials és un d'ells i es tracta d'un important aspecte per disminuir els grans costos i recursos que una missió espacial implica, minimitzant també l'impacte ambiental.

Aquest treball desenvolupa l'estudi i la implementació del control per la recuperació segura dels sistemes de llançament d'un coet.

Per tal d'assolir aquest anàlisis, s'avaluen els actuals coets reutilitzables, seleccionant el Falcon 9 del SpaceX com a model principal en el qual el projecte es centra. Un cop caracteritzat aquest sistema en particular, es determina la modelització d'equacions del problema amb l'objectiu de crear un programa en l'entorn de Matlab i efectuar simulacions.

La necessitat d'un sistema de control és inferida mitjançant els resultats de les primeres simulacions a causa de l'absència dels paràmetres d'aterratge segur, d'entre els quals el més important és una velocitat final pròxima a 0. Conseqüentment, es proposen i comparen diferents controladors lineals a fi d'aconseguir el comportament desitjat del sistema. No obstant, les no-linealitats del problema sumades a les limitacions d'aquests controladors incrementa la complexitat, a causa de la considerable quantitat d'entrades de control. Per aquests motius, el sistema es simplifica englobant les forces i els moments en les corresponents resultants amb les quals la totalitat de les superfícies de control han de contribuir. Seguint aquesta metodologia, el sistema desenvolupat consisteix en controlar la velocitat mitjançant les forces i l'angle de capcineig amb els moments. D'aquest últim, s'extreu com a conclusió que el Control Predictiu basat en Model disposa d'una tendència a ajustar-se millor a la consigna que el PID.

En definitiva, les limitacions d'aquests controladors tenen un impacte en la resposta final i, per aquesta raó, es requereixen de propostes més complexes per tal d'adquirir una aproximació encara més propera al problema real, com per exemple controladors no lineals o un segon nivell d'aquests per determinar les accions que cada dispositiu de control haurien d'efectuar a partir de les resultants de les forces i els moments, les quals són les entrades del sistema que ja ha estat controlat.

Acknowledgements

Behind this thesis are hours of research and work, which gives a closure to four years of struggle and effort.

During the development of the project I have had the unconditional support of my thesis director, Fatiha Nejjari, whom I thank for the help and advices proportioned to me.

I would like to thank my family for standing always by my side and cheering me up whenever I needed. Specially, to my parents for helping me to pursue and accomplish my goals and my dreams, to my siblings for aiding me despite being far apart, and to the little ones, Erik and Derek, for giving me strength to try setting a good example for them.

To my friends, the ones that has always been there and the ones that I have been able to know these years, thank you for understanding me better than anyone and keeping me going day by day.

Thank you all, for being there.

Contents

List of Figures

List of Tables

List of symbols and abbreviations

Reference frames

O_b	Origin of the body reference frame
x_b	x-axis of the body reference frame
y_b	y-axis of the body reference frame
z_b	z-axis of the body reference frame
O_e	Origin of the Earth reference frame
x_e	x-axis of the Earth reference frame
y_e	y-axis of the Earth reference frame
z_e	z-axis of the Earth reference frame
O_h	Origin of the local horizon reference frame
x_h	x-axis of the local horizon reference frame
y_h	y-axis of the local horizon reference frame
z_h	z-axis of the local horizon reference frame
O_w	Origin of the wind reference frame
x_w	x-axis of the wind reference frame
y_w	y-axis of the wind reference frame
z_w	z-axis of the wind reference frame
L_{be}	Transformation matrix from Earth-frame to body-frame
L_{bw}	Transformation matrix from wind-frame to body-frame

General formulation

$\vec{F}$	Forces vector
$\vec{M}$	Moments vector
$\vec{h}$	Angular momentum vector
$\vec{\Omega}$	Absolute angular velocity
I	Inertia tensor

I_{ij}	Inertia within the i and j component

Masses

m	Instantaneous mass of the first stage
m_0	Initial mass of the first stage
m_{st}	Dry mass of the first stage

Velocities

$\vec{\omega}$	Angular velocity
p	Angular velocity in x_b
q	Angular velocity in y_b
r	Angular velocity in z_b
$\vec{V}$	Linear velocity
u	Linear velocity in x_b
v	Linear velocity in y_b
w	Linear velocity in z_b

Euler angles

θ	Pitch angle
ϕ	Roll angle
ψ	Yaw angle

Velocity angles

α	Angle of attack
β	Sideslip angle

Gravity forces

g	Gravity
g_0	Standard gravity

G	Universal gravitational constant
M	Earth mass
R_m	Earth radius
z	Geometric altitude
$h(z)$	Geopotential altitude

Thrust

T	Thrust module
I_{sp}	Specific impulse of the engines
ε_z	Angle of the thrust respect to its projection to the $x_b - y_b$ plane
ε_x	Angle between the thrust projection to the $x_b - y_b$ plane and the x_b axis
x_{cm}	Distance between the thrust application point and the centre of mass

Aerodynamic forces

C_L	Lift force coefficient
C_D	Drag force coefficient
L	Lift force
D	Drag force
S	Reference area
ρ	Air density
d_{CP}	Distance between the centre of mass and the centre of pressure
x_{cp}	Distance between the base of the stage and the centre of pressure

Cold gas thrusters forces

T_{N_2}	Cold gas thrusters force module
ν_z	Angle of the cold gas thrusters force respect to its projection to the $x_b - y_b$ plane

ν_x	Angle between the cold gas thrusters force projection to the $x_b - y_b$ plane and the x_b axis
$d_{T_{N_2}}$	Distance from the centre of mass to the cold gas thrusters force application in x_b direction
R_{st}	Distance from the centre of mass to the cold gas thrusters force application in y_b direction

Grid fins forces

M	Mach number
a	Sound velocity
α_{eff}	Effective angle of attack
δ	Fin deflection angle
$C_{N,fin}$	Fin normal force coefficient
$C_{N\delta,fin}$	Initial lift-curve slope respect to the fin deflection
$C_{N\alpha}$	Initial lift-curve slope respect to the angle of attack
$C_{A,fin}$	Fin axial force coefficient
C_{Ai}	Fin induced drag coefficient
C_{Adp}	Fin pressure drag coefficient
C_{Ap}	Fin interference drag
C_{Af}	Fin skin friction drag
$S_{wet,fin}$	Fin wet area
$S_{ref,fin}$	Fin reference area
t	Fin thickness
c	Fin chord
$(np + 2)$	Fin intersection points
Re	Reynolds number
x	Charesteristic length
μ	Dynamic viscosity of the fluid

μ_0	Dynamic reference viscosity of the fluid
T	Temperature
T_0	Reference temperature
C_s	Sutherland's constant
N	Fin normal force
A	Fin axial force
r_{fin}	Distance from the centre of mass of the stage to fin forces application within $y_b - z_b$ plane
d_{fin}	Distance from the centre of mass of the stage to fin forces application along x_b axis

State space

X	State vector
U	Input vector
Y	Output vector

Control parameters

k_p	Proportional constant
k_i	Integral constant
k_d	Derivative constant

Abbreviations

DOF	Degree Of Freedom
COESA	Committee on Extension to the Standard Atmosphere
PID	Proportional Integral Derivative
MPC	Model Predictive Control

1 Introduction

Earth observation and outer space exploration is a relevant area of study that along the course of time has raised the technological advances within the aerospace industry. In order to carry out these missions, the introduction of improvements into the rockets devices has been a key factor to accomplish further objectives, being the recovery of their launch systems one of the current subject of matter.

1.1 Aim of the project

The principal aim of the project is to develop a successful control system for the recovery of the launch system of a rocket, ensuring a safe and achievable landing.

1.2 Scope

The main aspects within the scope of this project are defined below:

- Analyse successful rocket systems recoveries.
- Model a recovery system considering the different phases of the manoeuvre.
- Create a framework to simulate the landing conditions.
- Study the control of the system with different methods.
- Select the optimal control system.

It is important to mention that the project is focused on identifying the optimum control method by evaluating the currently existing control techniques and system modelling. Moreover, this study is limited to simulations due to the inaccessibility of physical assessments on real rockets of these magnitudes.

1.3 Requirements

The fundamental requirement of the project is to implement the objectives previously stated with an efficient method and pursuing its optimal performance.

Besides that, the technical and administrative requirements are listed below:

- Obtain a control adaptable for different orbital rocket launch systems by adjusting the inputs of the framework.
- The overall model within the simulation has to be implemented thorough an accurate theoretical basis in order to reach the most precise result.
- Develop the framework with MATLAB environment.
- Fulfil the project delivery date the 22nd of June 2021.

1.4 Justification

The continuous search of sources of life farther from Earth in addition to understanding the space environment have been a continuous investigation for mankind and, throughout the course of the space missions over the years, the advances in space technology are increasing promptly.

For this reason, the development of rockets in order to transport payload or people to an Earth orbit or even beyond our planet has been an area of concern that reaches to the present.

Nevertheless, the most relevant restriction is the huge cost that implicate completing a mission of these dimensions, which can easily extent over millions of euros.

Reusable launch systems of the rockets has become a recent subject of interest, since it implies a considerable decrease in the overall budget because these equipments can be used in further missions [1].

However, there are not a large number of satisfactory recoveries accomplished due to the complexity of this problem [2]. The main difficulty consists in preserving the calculated landing trajectory. Moreover, the estimation of this path has to take into account the perturbations to which this reusable launch system is subjected.

Hence, the essence of this project remains within the acquirement of additional information in this field by analysing for the control in order to develop an adequate method for achieving this manoeuvre.

1.5 Schedule

Once the scope and requirements are determined, the organisation of the tasks to accomplish them can be detailed.

Firstly, the work breakdown structure (WBS), which is a deliverable-oriented hierarchical decomposition of the work to be executed in order to accomplish the project objectives and create the required deliverables, is presented.

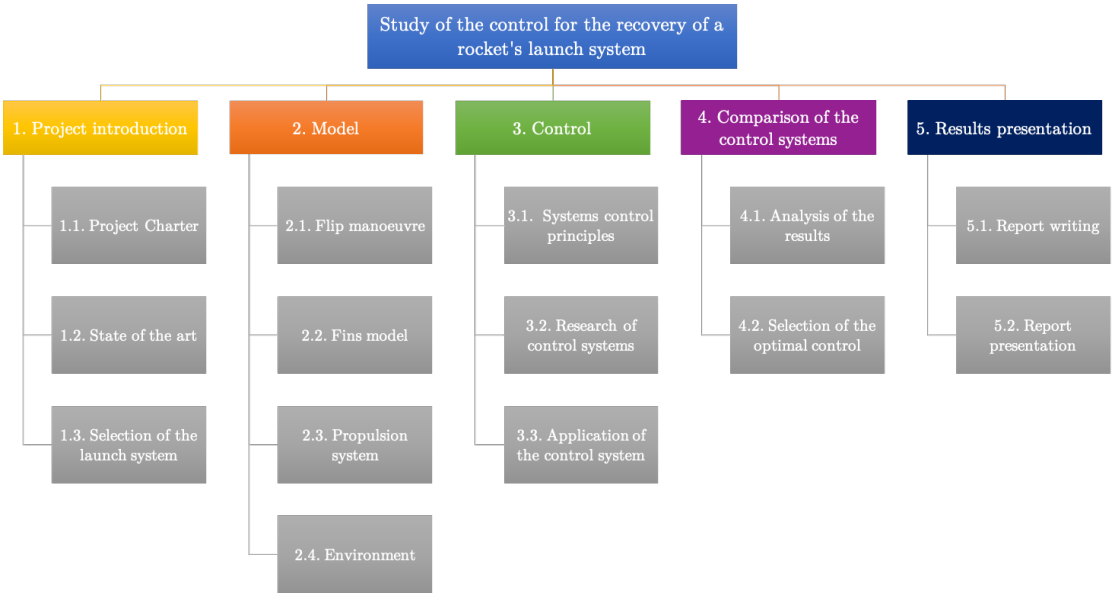

Figure 1: Work breakdown structure

Consequently, from the preceding diagram, the tasks are defined:

1. Project introduction: In the first group of tasks, the bases of the project are determined, presenting the field of research.

    1.1. Project Charter: Elaboration of this document, the initial deliverable, which includes the aim, justification, scope, requirements and schedule of the project.

1.2. State of the art: Search of the developments within the successful recoveries of the rockets.

1.3. Selection of the launch system: Once different rockets has been studied, one of their launch systems is selected in order to analyse its model and, subsequently, its control.

2. Model: Study the equations attached to the landing manoeuvre in order to model the system.

2.1. Flip manoeuvre: Model the first movement of the device once it is disengaged from the overall rocket, which consists in a flip to position the propulsion system towards the ground.

2.2. Fins model: Posterior to the flip manoeuvre, define the effect of the fins motion that adjust and maintain the trajectory into a vertical one.

2.3. Propulsion system: Analyse the final propulsion thrusters that decelerate the system.

2.4. Environment: Compute the possible perturbations produced by the landing conditions.

3. Control: Attempt to reach an accurate control of the recovery with different methodologies.

3.1. Systems control principles: Investigate the control theory in order to acknowledge the key factors within this area of study.

3.2. Research of control systems: Once the control basis are learnt, investigate the different control techniques.

3.3. Application of the control system: Implement the previous control methods through the model system.

4. Comparison of the control systems: Examine the responses of all the control systems and compare them.

    4.1. Analysis of the results: Detect the differences between each control system.

    4.2. Selection of the optimal control: Choose the most effective and optimal control system for the problem.

5. Results presentation: Write the documents that must be delivered which involve the overall work of the project.

    5.1. Report writing: Create the main project document which includes all the tasks developments.

    5.2. Report presentation: Elaborate the project presentation which summarise the report.

Consequently, the expected order of tasks and their level of effort estimation can be detailed through the next table:

Table 1: Tasks dependency and level of effort estimation

Code of task	Task identification	Preceding task	Level of effort [h]
1.	Project introduction	-	35
1.1.	Project Charter	-	20
1.2.	State of the art	-	10
1.3.	Selection of the launch system	1.2.	5
2.	Model	1.3.	130
2.1.	Flip manoeuvre	1.3.	30
2.2.	Fins model	2.1.	40
2.3.	Propulsion system	2.2.	20
2.4.	Environment	1.3.	40
3.	Control	2.4.	130
3.1.	Systems control principles	2.4.	25
3.2.	Research of control systems	3.1.	25
3.3.	Application of the control system	3.2.	80
4.	Comparison of the control systems	3.3.	30
4.1.	Analysis of the results	3.3.	20
4.2.	Selection of the optimal control	4.1.	10
5.	Results presentation	-	130
5.1.	Report writing	-	100
5.2.	Report presentation	5.1.	30

Finally, with the previous table, the gantt chart is sketched below:

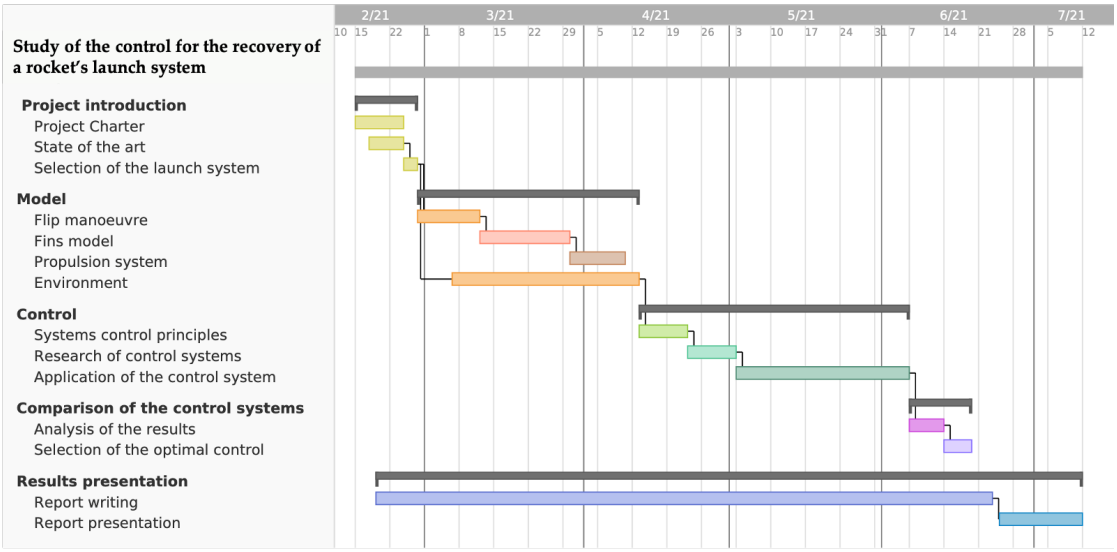

Figure 2: Gantt chart of the project

2 State of the art

In this section, the current developments within the recovery technologies applied to the rockets are described.

2.1 Parachutes recovery

The first attempts to fulfil this objective consisted in the deployment of parachutes in order to brake the system and accomplish a safe landing, usually in the water.

However, there is a significant guidance uncertainty with the use of the parachute systems, which imply an unsuitable accuracy of the control that inhibit the possibility to land on exact coordinates. For this reason, this type of recovery is generally implemented in small rockets or water landings, the recovery of which is carried out by a ship approaching its location. The last case possess a susceptibility to require a reconditioning for the structure, due to the damage that the salt water can cause to the electrical components. Nevertheless, it is usually employed on the landing of crewed capsules, since it is safer for the integrity of the inside passengers [3].

For instance, Rocket Lab, a private American aerospace manufacturer, recently developed a reusable rocket whose first stage is retrieved by landing on water with parachutes [4]. Moreover, NASA has implemented this type of recoveries in several missions, mainly in the crewed capsules.

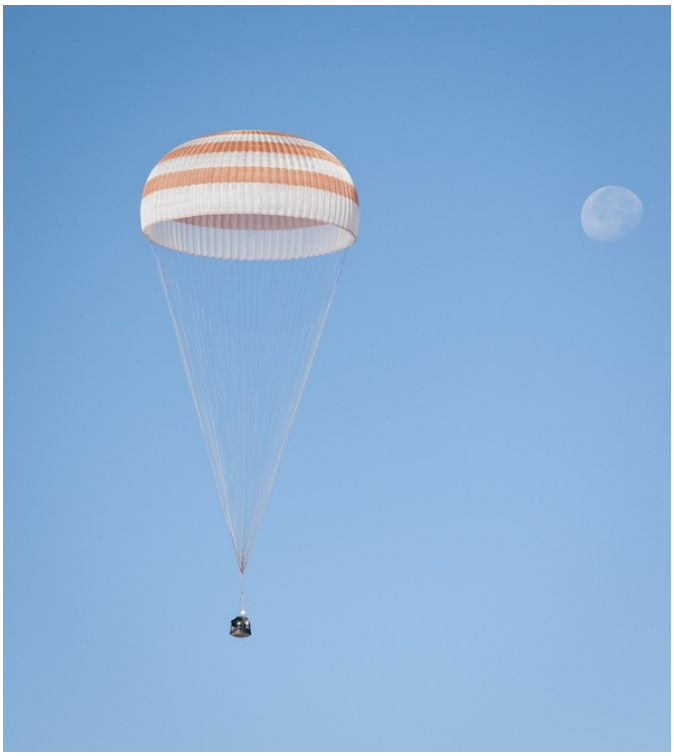

Figure 3: Soyuz capsule landing [5]

2.2 Vertical landing recovery

The latest technique is performed by the propulsion systems to decelerate the structure accomplishing a vertical landing on ground or on a platform in the sea. Thus, in this case the thrusters allow a more precise control, which also increase the complexity.

The first successful recovery with this methodology was implemented by the American company Blue Origin, accomplishing the first booster landing, which is the first stage of a multistage launch vehicle named New Shepard. Nevertheless, it consisted in a suborbital performance, achieving a maximum altitude of 101.7 kilometers by the capsule of the spacecraft [6].

Despite the precedent case, the American private business SpaceX is currently interested in this type of recovery and has operated it successfully for the first

stage of the Falcon 9 rocket on a drone ship and also for boosters of the Falcon Heavy on ground [7].

(a) First stage recovery of the Falcon 9 on a drone ship

(b) Boosters recovery of the Falcon Heavy on ground

Figure 4: Vertical landing revovery from SpaceX [7]

2.3 Other recoveries

In addition, aside from the previous methods, there are other parts of the spacecraft that can be retrieved and reused, such as the fairing. Along the lines of the example from the previous subsection, SpaceX has carried out some fairing recoveries successfully.

This process involves the separation into two halves of the fairing, each of which was controlled by steering thrusters and parachutes, and the posterior retrieval by two large catching nets at sea. Nonetheless, as aforementioned, the instability from the control of the parachutes adds complications and is the reason why barely less than the 30% of the landings were achieved [8].

Figure 5: Fairing recovery of the Falcon 9 [7]

3 Problem description

The present section introduces the case of study, in which the project is centred, by justifying its selection and analysing the associated manoeuvres of the landing performance.

3.1 System selection

Once the current developments are presented in the precedent section, the parachute recovery and the vertical landing are consistent candidates for the aim of the project. Nonetheless, the first technique, as aforementioned, has certain margin of error and this is the reason why the vertical landing recovery is selected.

From the overall successful performances implementing this method of the different aerospace manufacturers, the ones stated in section 2.2 are among the most relevant.

Hence, studying each methodology, both corporations have numerous dissimilarities. Firstly, the control subsystems of the first stage of the New Shepard from Blue Origin consisted in four deployable wedge fins and thrust vectoring control, which provides the ability of adjusting the direction of the thrust from the engine.

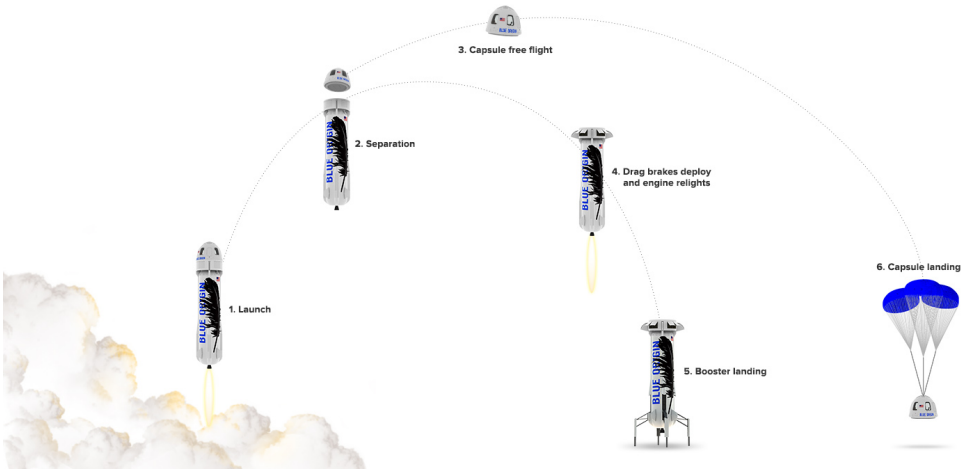

Figure 6: New Shepard trajectory performance [9]

Despite this, as exposed previously, it particularly accomplished a suborbital retrieval and, consequently, does not fulfil the established requirements. Therefore, the SpaceX is the case of study because of its compliance with both the scope and requirements of the project.

Specifically, the Falcon 9 is selected, since the Falcon Heavy is formed of the precedent one as the centre core and two additional similar to its first stage as strap-on boosters. Furthermore, the studied version of the rocket is v1.2 Block 5, the most recent one. Regardless, as stated in the requirements, the developed framework can be modified by any orbital rocket which is capable of performing this type of manoeuvre, detailed in the next subsection.

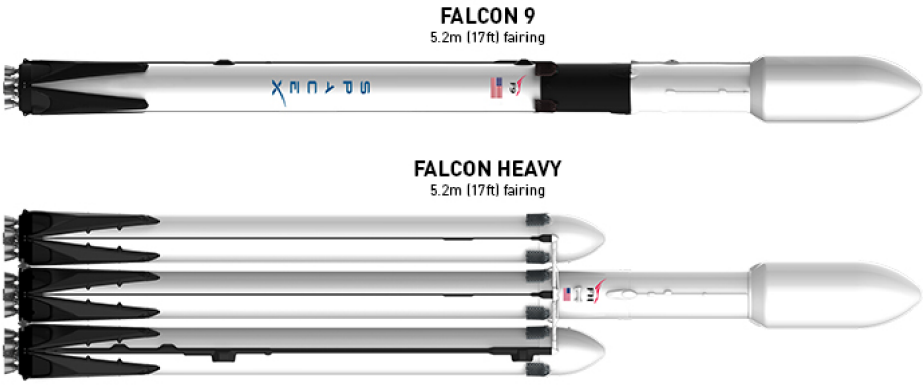

Figure 7: Falcon 9 and Falcon Heavy [7]

3.2 Vehicle overview

Falcon 9 is an orbital rocket formed of two stages and the latest version, v1.2 Block 5, has an overall height of 70 m and a total mass of 549,054 kg. Regarding the first stage, on which the project is focused, it possesses the characteristics summarised below:

Table 2: Falcon 9 first stage dimensions and characteristics [10] [11]

Dimensions	
Height	47.50 m
Diameter	3.66 m
Masses	
Dry mass	22,200 kg
Wet mass	433,100 kg
Propulsion	
Engine type	Liquid, gas generator
Engine designation	Merlin 1D (M1D)
Number of engines	9
Propellant	Liquid oxygen (LOX) / kerosene (RP-1)
Total thrust	7,686 kN (sea level)
Recovery accessories	
Cold gas thrusters	8 Nitrogen gas thrusters
Fins	4 hypersonic grid fins
Landing gear	4 lightweight landing legs

The main components of the recovery system are the engines, the cold gas thrusters, the fins and the landing gear. First of them, consist in nine Merlin 1D engines with up to 854 kN thrust per engine at sea level. These are gimbaled engines, which provides the rocket with a thrust vectoring system, and their arrangement consists in an octaweb configuration, in other words, a central engine and alongside it forming a circle the others eight remaining.

Figure 8: Falcon 9 first stage octaweb engines [7]

Next in order, the nitrogen gas thrusters and the fins are situated at the top of the first stage, that corresponds to the base of the interstage, which connects the first and second stages and houses the pneumatic pushers that allow their separation during flight. In figure 9, the interstage can be seen, which is the black part, and also these control systems.

The cold gas thrusters are grouped in two pods symmetrically placed, each of which dispose of four thrusters for different directions. In addition, the four hypersonic grid fins, that are movable permitting to orient the rocket during reentry by relocating the centre of pressure, are also symmetrically positioned and the nitrogen thrusters are located in the middle of two fins at opposite sides.

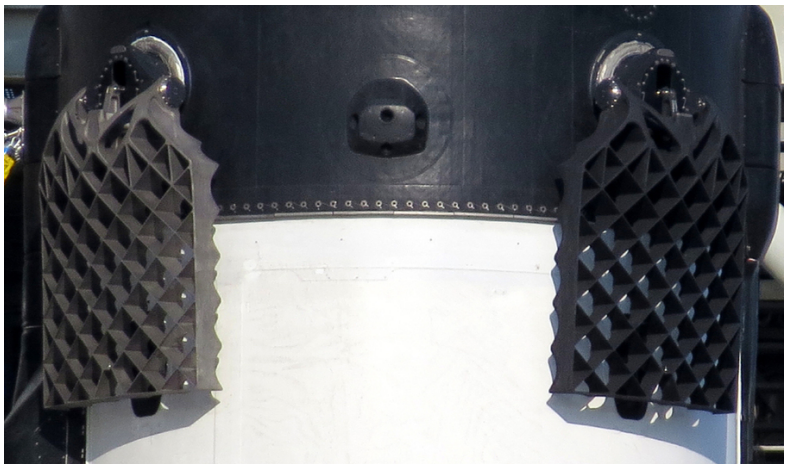

Figure 9: Falcon 9 cold gas thrusters at the centre and the grid fins at both sides [12]

The last of them, the landing gear, consist on four deployable landing legs symmetrically distributed at the base of the first stage.

Figure 10: Falcon 9 landing gear [7]

3.3 Conceptual definition

Deepening in its first stage recovery, the landing process can be divided into three main manoeuvres: the flip manoeuvre, the fins deployment and the vertical landing.

Starting off, once the landing stage is separated from the whole spacecraft and its engines are shut down, the cold gas thrusters are triggered to rotate the stage in the trajectory plane in order to accomplish an horizontal position with the engine leading the movement.

Afterwards, the central engine and up to two more are reignited, since it is required to brake the structure and align it into a descent path, and the grid fins are deployed with the purpose of moving them to achieve an approximate vertical position.

Finally, aiming to fulfil also the preceding objective, at the final approach to the drone ship, the central and two more engines through their thrust vectoring, as they are gimbaled engines, are activated and the landing gear is deployed, in the interest of decelerating the stage and, consequently, performing a safe landing.

To summarise, the overall recovery process can be sketched by the diagram below.

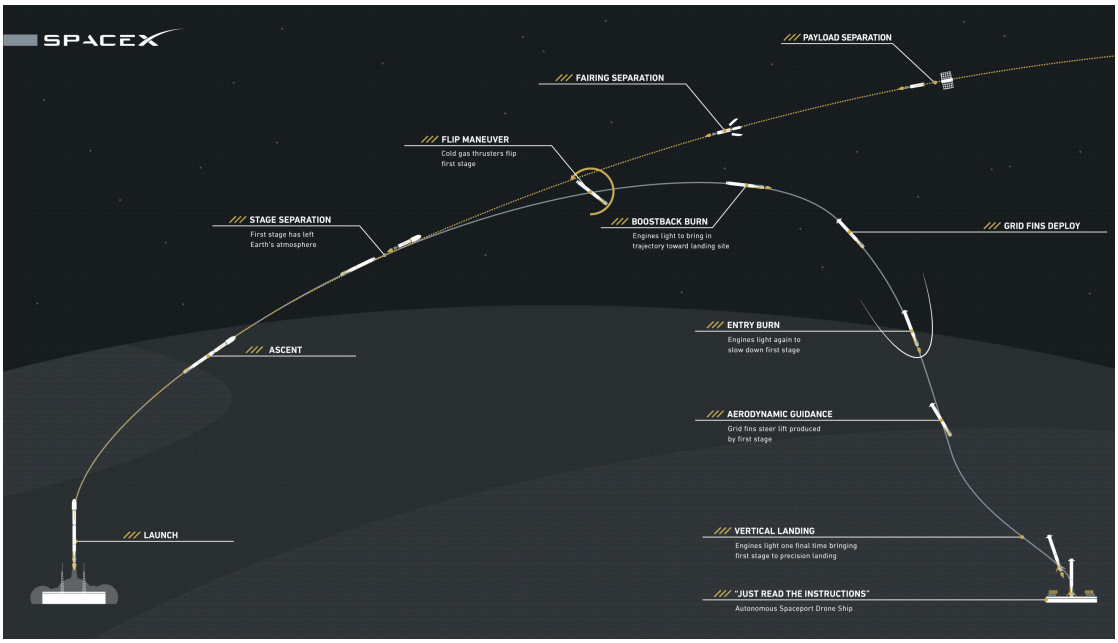

Figure 11: Sketch of the trajectory from the Falcon 9 performance [7]

Regarding the landing control of this first stage, it is equipped with an Inertial Navigation System (INS), which consist of several types of sensors that keep track of the position, orientation and velocity, and also with a Global Positioning System (GPS) to measure the geolocation. Hence, with the real-time information of both INS and GPS, is compared against the pre-programmed flight path, instructing to correct the deviations if necessary by adjusting its orientation and velocity.

4 System modelling

Once the problem is stated and detailed, the modelling of the system is developed by describing the equations that dictate the overall landing manoeuvre, in order to implement them into a simulation framework.

4.1 Reference frames

Firstly, deepening in the different systems of frames in which the model will be referenced, first of them, the body axes (O_b, x_b, y_b, z_b) is centred in the centre of mass with the x_b and z_b directions within the symmetry plane of the structure pointing forward and downward, respectively, and y_b perpendicular to them. Secondly, the Earth axes (O_e, x_e, y_e, z_e) is a rotating Earth-centred system that has its origin in the planet surface with z_e axis directed to Earth centre, x_e to the north within the horizontal plane and y_e to the east.

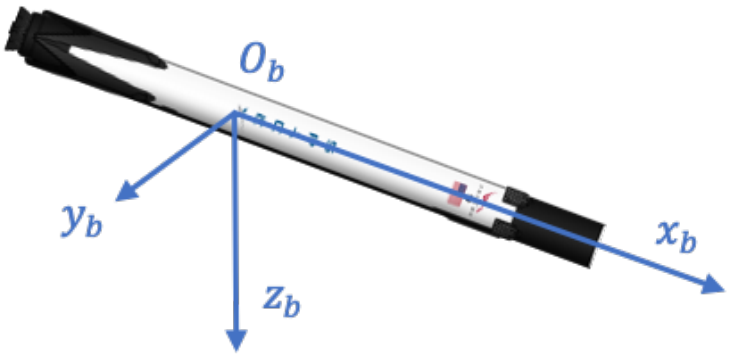

Figure 12: Body axes, first stage drawing from [7]

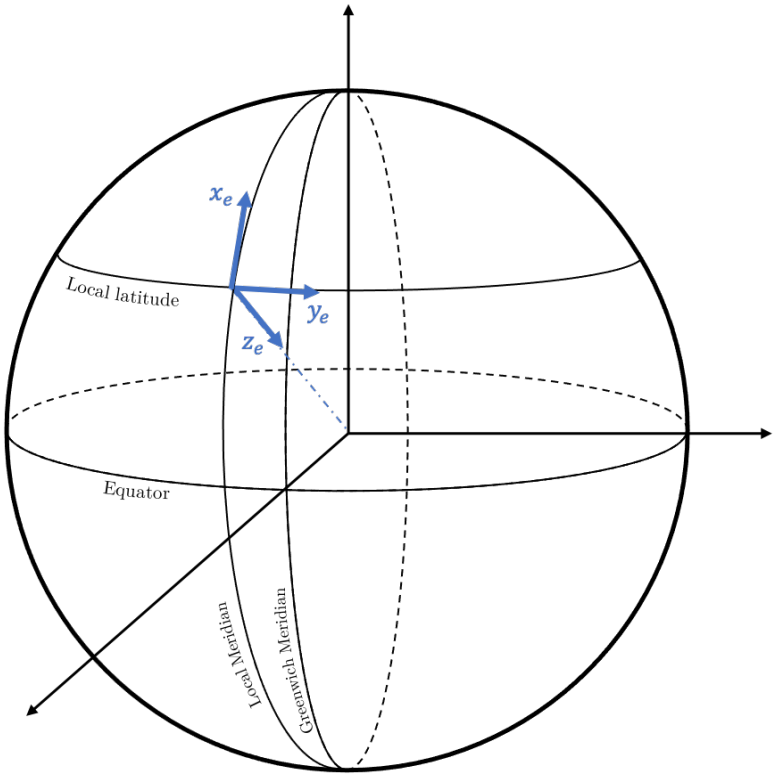

Figure 13: Earth axes sketch

In order to change the reference from Earth-frame to body-frame, or vice versa, the orthonormal transformation matrix with the Euler rotation angles: pitch (θ), roll (ϕ) and yaw (ψ) [13], is used.

$$L_{be} = \begin{bmatrix} \cos\theta\cos\psi & \cos\theta\sin\psi & -\sin\theta \\ (-\cos\phi\sin\psi + \sin\phi\sin\theta\cos\psi) & (\cos\phi\cos\psi + \sin\phi\sin\theta\sin\psi) & \sin\phi\cos\theta \\ (\sin\phi\sin\psi + \cos\phi\sin\theta\cos\psi) & (-\sin\phi\cos\psi + \cos\phi\sin\theta\sin\psi) & \cos\phi\cos\theta \end{bmatrix} \quad (1)$$

For a better understanding, the sketch of the body reference system respect the local horizon (O_h, x_h, y_h, z_h), which is parallel to the Earth-frame, is attached below.

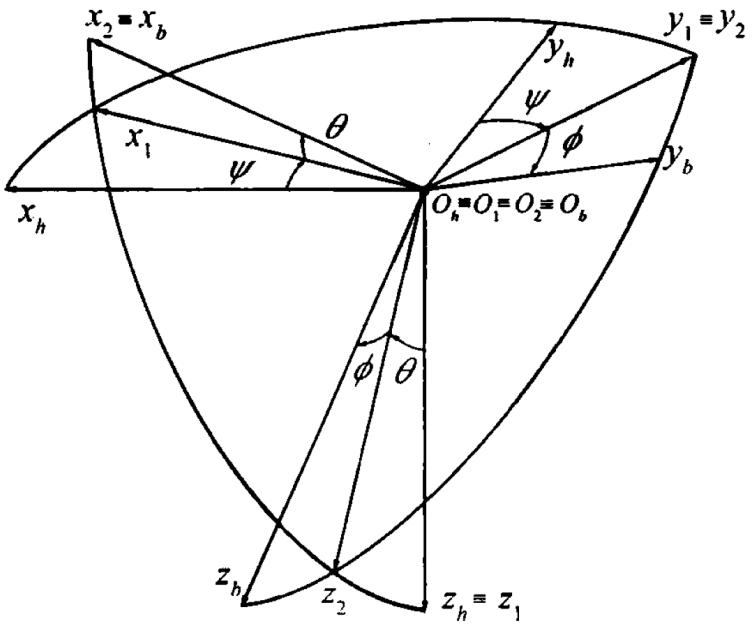

Figure 14: Body axes respect local horizon axes [13]

Moreover, an additional reference frame is needed in order to represent the aerodynamic forces, the wind-frame (O_w, x_w, y_w, z_w), whose origin is also in the centre of mass, the x_w axis is in the aerodynamic velocity of the body direction, the z_w is within the symmetry plane and perpendicular to the previous one and the remaining is the corresponding to obtain an orthogonal coordinate system. Therefore, by defining the angles α, and β as the angle of attack, and the sideslip angle, respectively, the transformation matrix is accomplished:

$$L_{bw} = \begin{bmatrix} \cos\alpha\cos\beta & -\cos\alpha\sin\beta & -\sin\alpha \\ \sin\beta & \cos\beta & 0 \\ \sin\alpha\cos\beta & -\sin\alpha\sin\beta & \cos\alpha \end{bmatrix} \tag{2}$$

And the representation of the wind reference system respect the body-frame is showed next.

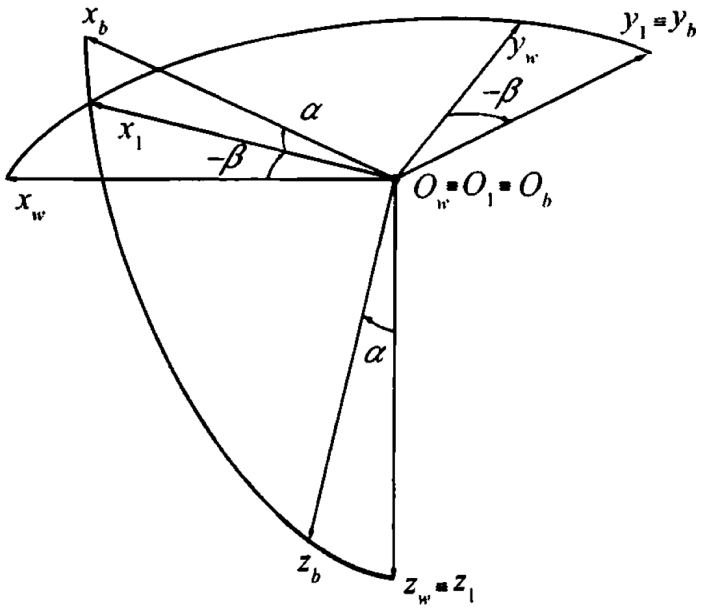

Figure 15: Wind axes respect body axes [13]

4.2 Model equations

Once the reference frames are defined, in reference to the physical problem, the rocket dynamic model is based in two fundamental theorems of Classical Mechanics: the linear momentum and the angular momentum theorems.

Starting off, the linear momentum conservation is expressed as the following:

$$\vec{F} = \frac{\mathrm{d}(m\vec{V})}{\mathrm{d}t} \tag{3}$$

being $\vec{F}$ the resultant of the external forces, $\vec{V}$ the velocity at the centre of mass (in inertial reference), m the mass and t the time.

In reference to the angular momentum theorem, it can be formulated as:

$$\vec{M} = \frac{\mathrm{d}\vec{h}}{\mathrm{d}t} \tag{4}$$

$$\vec{h} = I\vec{\Omega} \tag{5}$$

where $\vec{M}$ is the resultant of the exterior moments around the centre of mass, $\vec{h}$ is the total kinetic moment, $\vec{\Omega}$ is the absolute angular speed and I the inertia tensor, presented below:

$$I = \begin{bmatrix} I_{xx} & -I_{xy} & -I_{xz} \\ -I_{xy} & I_{yy} & -I_{yz} \\ -I_{xz} & -I_{yz} & I_{zz} \end{bmatrix} \tag{6}$$

In addition, due to the movement of the rocket along its trajectory, the forces of the system are simpler to represent respect to the body axes, which are attached to the mass and its movement, as seen in the previous subsection. Hence, given this rotational reference, since the results are desired to be represented in the Earth axes, which can be considered an inertial frame, the term that involves the angular speed of the body frame ($\vec{\omega}$) is required to be added.

$$\vec{F} = \frac{\partial\left(m\vec{V}\right)}{\partial t} + \vec{\omega} \times \vec{V} \qquad \vec{M} = \frac{\partial\vec{\omega}}{\partial t} + \vec{\omega} \times \vec{h} \tag{7}$$

From these equations, establishing that the angular and linear velocities vectors are the ones expressed next, the problem equations are developed based on references [13], [14], [15] and [16].

$$\vec{\omega} = \begin{bmatrix} p \\ q \\ r \end{bmatrix} \qquad \vec{V} = \begin{bmatrix} u \\ v \\ w \end{bmatrix} \tag{8}$$

Moreover, in order to take into account the Earth rotation, within the $\vec{\omega}$ parameter, the values of the planet angular speed (p_E, q_E, r_E, respectively) must be added.

Thus, by substituting these into equations (7) and decomposing into each axis,

the Euler's equations would be obtained :

$$\begin{aligned} F_{x_b} &= m(\dot{u} + qw - rv) \\ F_{y_b} &= m(\dot{v} + ru - pw) \\ F_{z_b} &= m(\dot{w} + pv - qw) \\ M_{x_b} &= I_{xx}\dot{p} - I_{xz}(\dot{r} + pq) + (I_{zz} - I_{yy})\, qr \\ M_{y_b} &= I_{yy}\dot{q} + I_{xz}\left(p^2 - r^2\right) + (I_{xx} - I_{zz})\, rp \\ M_{z_b} &= I_{zz}\dot{r} - I_{xz}(\dot{p} - qr) + (I_{yy} - I_{xx})\, pq \end{aligned} \tag{9}$$

And rearranging the terms, the next expressions are achieved:

$$\begin{aligned} \dot{u} &= \frac{F_{x_b}}{m} - (qw - rv) \\ \dot{v} &= \frac{F_{y_b}}{m} - (ru - pw) \\ \dot{w} &= \frac{F_{z_b}}{m} - (pv - qu) \end{aligned}$$

$$\dot{p} = \frac{I_{zz}M_{x_b}}{I_{xx}I_{zz} - I_{xz}^2} + \frac{I_{xz}M_{z_b}}{I_{xx}I_{zz} - I_{xz}^2} + \frac{(I_{xx} - I_{yy} + I_{zz})\, I_{xz}}{I_{xx}I_{zz} - I_{xz}^2}pq + \frac{(I_{yy} - I_{zz})\, I_{zz} - I_{xz}^2}{I_{xx}I_{zz} - I_{xz}^2}qr$$

$$\dot{q} = \frac{M_{y_b}}{I_{yy}} + \frac{I_{xz}}{I_{yy}}\left(r^2 - p^2\right) + \frac{I_{zz} - I_{xx}}{I_{yy}}pr$$

$$\dot{r} = \frac{I_{xz}M_{x_b}}{I_{xx}I_{zz} - I_{xz}^2} + \frac{I_{xx}M_{z_b}}{I_{xx}I_{zz} - I_{xz}^2} + \frac{(I_{xx} - I_{yy})\, I_{xx} + I_{xz}^2}{I_{xx}I_{zz} - I_{xz}^2}pq + \frac{(I_{yy} - I_{xx} - I_{zz})\, I_{xz}}{I_{xx}I_{zz} - I_{xz}^2}qr \tag{10}$$

It is important to remark that m is the instantaneous mass, hence the flow rate equation [17], which indicates the mass variance along time, is needed:

$$\dot{m} = -\frac{T}{g_0 I_{\text{sp}}} \tag{11}$$

being T the thrust module, g_0 the standard gravity acceleration and I_{sp} the specific impulse of the engines.

Furthermore, with the purpose of defining the position of the rocket, necessary to estimate the landing coordinates, the calculations are effectuated through the

Euler angles:

$$\begin{aligned} \dot{\theta} &= q\cos\phi - r\sin\phi \\ \dot{\phi} &= p + (q\sin\phi + r\cos\phi)\tan\theta \\ \dot{\psi} &= (q\sin\phi + r\cos\phi)\sec\theta \end{aligned} \tag{12}$$

And, with the transformation matrix (1), the motion respect to the Earth-frame can be expressed:

$$\begin{aligned} \dot{x}_E = u(\cos\theta\cos\psi) + v(\sin\phi\sin\theta\cos\psi - \cos\phi\sin\psi) \\ +w(\cos\phi\sin\theta\cos\psi + \sin\phi\sin\psi) \\ \dot{y}_E = u(\cos\theta\sin\psi) + v(\sin\phi\sin\theta\sin\psi + \cos\phi\cos\psi) \\ +w(\cos\phi\sin\theta\sin\psi - \sin\phi\cos\psi) \\ \dot{z}_E = u(-\sin\theta) + v(\sin\phi\cos\theta) + w(\cos\phi\cos\theta) \end{aligned} \tag{13}$$

Nevertheless, the Euler angles equations has a singularity in $\theta = \pm 90°$, which must be taken into account in its implementation.

Moreover, by solving the expressions from the linear velocities components within the system equations (10), its module (V), the angle of attack (α) and the sideslip angle (β), whose values are required in the transformation matrix (2), can be obtained.

$$\begin{aligned} V &= \sqrt{u^2 + v^2 + w^2} \\ \alpha &= \tan^{-1}\left(\frac{w}{u}\right) \\ \beta &= \tan^{-1}\left(\frac{u}{V}\right) = \sin^{-1}\left(\frac{v}{V}\right) \end{aligned} \tag{14}$$

Finally, aiming to complete the equations, in the next subsections the forces will be studied.

4.2.1 Gravitational forces

The weight of the mass consists in a vector that points to the Earth's centre of mass, thus, in order to represent it in the body axes, the transformation matrix

1 is applied, achieving the following forces:

$$\begin{aligned} F_{x(grav)} &= -mg\sin\theta \\ F_{y(grav)} &= mg\sin\phi\cos\theta \\ F_{z(grav)} &= mg\cos\phi\cos\theta \end{aligned} \tag{15}$$

where g would be the gravity acceleration, obtained from the gravity law:

$$g = \frac{GM}{r^2} \tag{16}$$

being G the universal gravitational constant, M the Earth mass and r the distance measured from the planet's centre of mass. Assuming an spherical Earth model, this last term is calculated by adding its radius (R_m) to the geopotential altitude of the problem body ($h(z)$), which accounts for the planet's mass attraction and the centrifugal effect of its rotation [18]:

$$r = R_m + h(z) \tag{17}$$

$$h(z) = \frac{R_m z}{R_m + z} \tag{18}$$

and z is the geometric altitude.

In reference to the moments, these forces are applied in the stage's centre of mass.

4.2.2 Thrust

Secondly, as stated in section 3, the gimbaled engines offers the possibility of adjusting the thrust force direction, and it can be represented with the angles ε_z, which is the angle of the thrust respect to its projection to the $x_b - y_b$ plane and ε_x, the angle between this projection and the x_b axis.

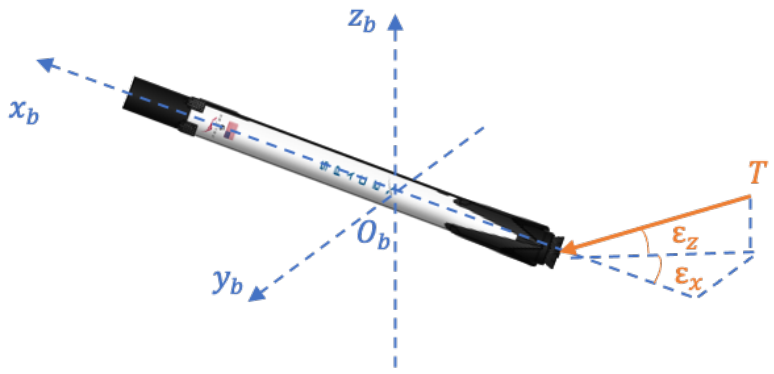

Figure 16: Thrust vector representation, first stage drawing from [7]

Thus, projecting into the body axes, the thrust force (T) would be decomposed by the expressions below:

$$\begin{aligned} T_x &= T\cos\varepsilon_z\cos\varepsilon_x \\ T_y &= T\cos\varepsilon_z\sin\varepsilon_x \\ T_z &= -T\sin\varepsilon_z \end{aligned} \tag{19}$$

And, in this case, the forces application is in the base of the stage, where the engines are located, considered along x_b axis and the distance between this point and the centre of mass is named x_{cm}.

4.2.3 Aerodynamic forces

Within the forces generated due to the aerodynamics influence, omitting the control accessories, it will be taken into account the research from [19], which offers the next lift and drag coefficients (C_L and C_D, respectively) approach:

$$\begin{aligned} C_L(\alpha) &= C_{L0} + C_{L\alpha}\alpha \\ C_D(\alpha) &= C_{D0} + C_{D\alpha}\alpha + C_{D\alpha^2}\alpha^2 \end{aligned} \tag{20}$$

where $C_{L0} = -0.2070$, $C_{L\alpha} = 1.676\,\text{rad}^{-1}$, $C_{D0} = 0.07854$, $C_{D\alpha} = -0.3529\,\text{rad}^{-1}$ and $C_{D\alpha^2} = 2.040\,\text{rad}^{-2}$, being α the angle of attack, in radians.

Hence, the lift and drag forces (L and D, respectively) can be accomplished

with the following equations:

$$L = \frac{1}{2}\rho(z)V^2SC_L(\alpha) \qquad D = \frac{1}{2}\rho(z)V^2SC_D(\alpha) \tag{21}$$

where V is the linear velocity (module of the vector $\vec{V}$), S the reference area and $\rho(z)$ the density for a given height z. Thus, the density model most suitable to the Standard Atmosphere Tables [20] is provided by the expression below:

$$\rho(z) = \rho_0 e^{-(z-R_m)/H} \tag{22}$$

being $\rho_0 = 1.225426\,\mathrm{kg/m^3}$ and $H = 7254.24\,\mathrm{m}$.

Finally, since these forces are within the wind-frame, the corresponding decomposition into the body axes through the transformation matrix (2) present the next contributions:

$$\begin{aligned} F_{x(aero)} &= L\sin\alpha - D\cos\alpha\cos\beta \\ F_{y(aero)} &= -D\sin\beta \\ F_{z(aero)} &= -L\cos\alpha - D\sin\alpha\cos\beta \end{aligned} \tag{23}$$

Due to the frame rotation, the directions of lift and drag forces are modified into their opposite whenever the pitch angle is higher to 90° and it must be taken into consideration.

And these forces are applied to the centre of pressure, which is considered along x_b axis and will be further analysed, and the length between the centre of mass and this is called d_{CP}.

Additionally to this aerodynamic forces, the ones from the landing control accessories are required to be computed.

4.2.4 Cold gas thrusters

Studying each recovery accessories, beginning with the nitrogen thrusters, it is relevant to establish that the body-frame is attached to the body by means that

the symmetry plane contains the two gas pods of each side.

Deepening into its functioning, each pod is able to eject nitrogen at both sides within the transverse plane of the stage, perpendicular to this and downwards to the landing legs position.

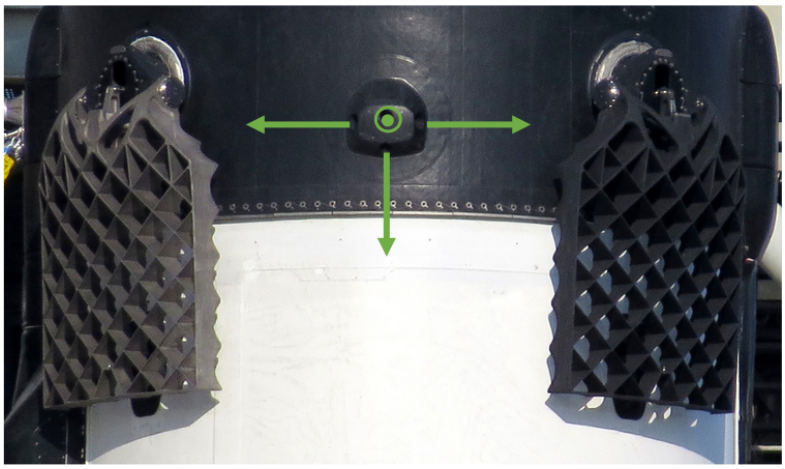

Figure 17: Sketch of the four directions of the nitrogen gas pod, photography from [12]

Therefore, likewise the thrust analysis, the resultant force vector can be expressed with two angles, ν_z and ν_x, which represent the angle between the the vector and its projection to the $x_b - y_b$ plane and the one between this projection and the x_b direction, respectively.

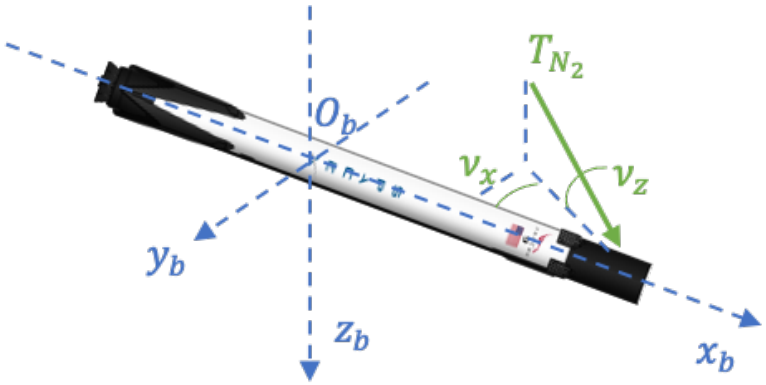

Figure 18: Nitrogen gas thrust vector representation, first stage drawing from [7]

Consequently, considering two vectors at each side, ${T_{N_2}}^{(1)}$ and ${T_{N_2}}^{(2)}$, with its corresponding angles and being the first the one represented above, the contributions along the body axes would be:

$$\begin{aligned} T_{x,N_2} &= T_{N_2}^{(1)} \cos\nu_z^{(1)} \cos\nu_x^{(1)} + T_{N_2}^{(2)} \cos\nu_z^{(2)} \cos\nu_x^{(2)} \\ T_{y,N_2} &= T_{N_2}^{(1)} \cos\nu_z^{(1)} \sin\nu_x^{(1)} - T_{N_2}^{(2)} \cos\nu_z^{(2)} \sin\nu_x^{(2)} \\ T_{z,N_2} &= T_{N_2}^{(1)} \sin\nu_z^{(1)} + T_{N_2}^{(2)} \sin\nu_z^{(2)} \end{aligned} \tag{24}$$

And the moments would be calculated taking into account the distances from the centre of mass to these forces applications, within the x_b and y_b directions, which corresponds to $d_{T_{N_2}}$ and the stage radius R_{st}, respectively.

4.2.5 Grid fins

Regarding the grid fins, the forces that produce can be expressed in terms of normal and axial forces, which in this case are applied in the centre of mass of the fins.

Besides this, the normal component behaviour is modified depending on whether the speeds at which the stage acquires are supersonic ($1.4 < M < 5$, being M the Mach number, $\frac{V}{a}$, and a the sound speed) or subsonic ($0 < M < 0.8$), and within the range of transonic velocities ($0.8 < M < 1.4$) these fins have nearly null effect.

Thus, for the supersonic scenario, the fin normal force coefficient, $C_{N,fin}$, is defined with the equation bellow, from [21]:

$$C_{N,fin} = \left.\frac{\delta C_{N\delta,fin}}{1+\frac{\delta}{\delta_{\max}}}\right|_{\alpha_{\text{eff}}=0} + \left.\frac{\alpha_{\text{eff}} C_{N\alpha}}{1+\frac{\alpha_{\text{eff}}}{\alpha_{\text{eff,max}}}}\right|_{\delta=0} \cdot \left(1 - \left.\frac{\delta C_{N\delta,fin}}{1+\left(\frac{\delta}{\delta_{max}}\right)^2}\right|_{\alpha_{\text{eff}}=0}\right) \tag{25}$$

where α_{eff} is the effective angle of attack, δ the fin deflection angle, $C_{N\delta,fin}$ is the initial lift-curve slope with respect to this fin deflection, which is estimated to

be 0.020 with a numerical study from [22], and $C_{N\alpha}$ has an analogue definition to the prior parameter but with respect to the angle of attack and is considered to be 0.067 [23]. Moreover, α_{eff} is considered to be sum of the real angle of attack and the fin deflection $(\alpha + \delta)$.

Secondly, for the subsonic case, the employed expression, from reference [24], is the following:

$$C_{N,fin} = \frac{C_{N\alpha}\alpha_{\text{eff}}}{(1 + K_1{\alpha_{\text{eff}}}^2)} \tag{26}$$

being the constant $K_1 = \frac{\pi}{6}$ with the result in radians.

And this value is corrected as a function of the Mach number (M):

$$(C_N)_{\text{at}M} = (C_N)_{\text{at}M=0} \cdot \left(1 - M^2\right)^{1/6} \tag{27}$$

In contrast, the axial force coefficient $(C_{A,fin})$ can be computed under the same functions for both supersonic and subsonic speeds [21]:

$$\begin{aligned} C_{Ai} &= C_{N,fin}\tan(\delta) \\ C_{Adp} &= \frac{S_{wet,fin}t}{2{\cdot}S_{ref,fin}c} \\ C_{Ap} &= 2 \cdot 0.000547 \cdot (np + 2) \end{aligned} \tag{28}$$

where C_{Ai} is the induced drag, which is produced due to fin deflection angle, C_{Adp} is the pressure drag, $S_{wet,fin}$ is the wet area, $S_{ref,fin}$ the reference area, t the fin thickness, c its chord and C_{Ap} the interference drag due to the fin element intersection points, that are defined as $(np + 2)$.

In addition, the skin friction drag, C_{Af}, is also required and can be approached discerning between laminar or turbulent flow:

$$C_{Af,\text{lam}} = \frac{0.664}{\sqrt{\text{Re}_x}} \qquad C_{Af,\text{turb}} = \frac{0.027}{\text{Re}_x^{1/7}} \tag{29}$$

where Re is the number of Reynolds defined as $\text{Re}_x = \frac{\rho v x}{\mu}$, being v the flow speed, x the characteristic length and μ the dynamic viscosity of the fluid. The

last parameter is calculated through the Sutherland's law [25]:

$$\mu = \mu_0 \left(\frac{T_0 + C_s}{T + C_s}\right) \left(\frac{T}{T_0}\right)^{\frac{3}{2}} \tag{30}$$

being μ the reference viscosity, T the temperature, T_0 the reference temperature and C_s the Sutherland's constant. For the studied case, since the fluid in which the rocket moves is the air, the preceding terms adopt the following values:

$$\mu_0 = 1.716 \cdot 10^{-5} \frac{\text{kg}}{\text{m} \cdot \text{s}} \qquad T_0 = 273.15\,\text{K} \qquad C_s = 110.4\,\text{K}$$

It is important to mention that for Re $\leq$ 2300 is considered laminar flow and for Re $\geq$ 3000 turbulent [26], however, with the purpose of simplifying the problem, the transitional flow is not contemplated, extending the laminar influence up to 2500 and considering greater values as turbulent.

Hence, the total coefficient is the total summation of the preceding ones:

$$C_A = C_{Ai} + C_{Af} + C_{Adp} + C_{Ap} \tag{31}$$

As it can be observed, this coefficient is estimated to be independent of the angle of attack, since it does not vary considerably along it.

Finally, the forces N and A, would be obtained through the next definitions:

$$N = \frac{1}{2}\rho(z)v^2 S C_N(\alpha, \delta) \qquad A = \frac{1}{2}\rho(z)v^2 S C_A \tag{32}$$

And taking into account the arrangement respect to the body axes, whose $x_b - y_b$ plane is at 45 degrees to both consecutive fins, in other words, it is in the middle of the them, the respective contributions for each one (from 1 to 4, in the x_b positive spin direction beginning from y_b) are determined:

$$\begin{aligned} F_{x(fins)} &= N^{(1)} + N^{(2)} + N^{(3)} + N^{(4)} \\ F_{y(fins)} &= \tfrac{\sqrt{2}}{2}\left(A^{(1)} - A^{(2)} - A^{(3)} + A^{(4)}\right) \\ F_{z(fins)} &= \tfrac{\sqrt{2}}{2}\left(A^{(1)} + A^{(2)} - A^{(3)} - A^{(4)}\right) \end{aligned} \tag{33}$$

In addition, for the moments computation, the distance from the centre of mass of the stage to these forces application within $y_b - z_b$ plane is named r_{fin} and along x_b axis d_{fin}.

4.3 State variable representation

To summarise the overall equations that involve the model of the system, the state space representation is used with the state vector (X), the input vector (U) and the output vector (Y), where:

$$X = [\, u \; v \; w \; p \; q \; r \; m \; \theta \; \phi \; \psi \; x_E \; y_E \; z_E \,]$$

$$U = \left[T \; \varepsilon_z \; \varepsilon_x \; T_{N_2}^{(1)} \; \nu_z^{(1)} \; \nu_x^{(1)} \; T_{N_2}^{(2)} \; \nu_z^{(2)} \; \nu_x^{(2)} \; \delta^{(1)} \; \delta^{(2)} \; \delta^{(3)} \; \delta^{(4)} \right] \tag{34}$$

$$Y = [\, u \; v \; w \; \theta \; \phi \; \psi \; x_E \; y_E \; z_E \; \dot{x}_E \; \dot{y}_E \; \dot{z}_E \;]$$

Consequently, the state space model, which consists in the derivative with respect to time of the state vector $(\dot{X})$, is expressed below:

$$
\begin{cases}
\dot{x_1} = \frac{F_{x_b}}{x_7} - (x_5 x_3 - x_6 x_2) \\
\dot{x_2} = \frac{F_{y_b}}{x_7} - (x_6 x_1 - x_4 x_3) \\
\dot{x_3} = \frac{F_{z_b}}{x_7} - (x_4 x_2 - x_5 x_1) \\
\dot{x_4} = \frac{I_{zz} M_x}{I_{xx} I_{zz} - I_{xz}^2} + \frac{I_{xz} M_z}{I_{xx} I_{zz} - I_{xz}^2} + \frac{(I_{xx} - I_{yy} + I_{zz}) I_{xz}}{I_{xx} I_{zz} - I_{xz}^2} x_4 x_5 + \frac{(I_{yy} - I_{zz}) I_{zz} - I_{xz}^2}{I_{xx} I_{zz} - I_{xz}^2} x_5 x_6 \\
\dot{x_5} = \frac{M_y}{I_{yy}} + \frac{I_{xz}}{I_{yy}} (x_6^2 - {x_4}^2) + \frac{I_{zz} - I_{xx}}{I_{yy}} x_4 x_6 \\
\dot{x_6} = \frac{I_{xz} M_x}{I_{xx} I_{zz} - I_{xz}^2} + \frac{I_{xx} M_z}{I_{xx} I_{zz} - I_{xz}^2} + \frac{(I_{xx} - I_{yy}) I_{xx} + I_{xz}^2}{I_{xx} I_{zz} - I_{xz}^2} x_4 x_5 + \frac{(I_{yy} - I_{xx} - I_{zz}) I_{xz}}{I_{xx} I_{zz} - I_{xz}^2} x_5 x_6 \\
\dot{x_7} = -\frac{u_1}{g_0 I_{\text{sp}}} \\
\dot{x_8} = x_5 \cos x_9 - x_6 \sin x_9 \\
\dot{x_9} = x_4 + (x_5 \sin x_9 + x_6 \cos x_9) \tan x_8 \\
\dot{x_{10}} = (x_5 \sin x_9 + x_6 \cos x_9) \sec x_8 \\
\dot{x}_{11} = x_1(\cos x_8 \cos x_{10}) + x_2(\sin x_9 \sin x_8 \cos x_{10} - \cos x_9 \sin x_{10}) \\
\qquad + x_3(\cos x_9 \sin x_8 \cos x_{10} + \sin x_9 \sin x_{10}) \\
\dot{x}_{12} = x_1(\cos x_8 \sin x_{10}) + x_2(\sin x_9 \sin x_8 \sin x_{10} + \cos x_9 \cos x_{10}) \\
\qquad + x_3(\cos x_9 \sin x_8 \sin x_{10} - \sin x_9 \cos x_{10}) \\
\dot{x}_{13} = x_1(-\sin x_8) + x_2(\sin x_9 \cos x_8) + x_3(\cos x_9 \cos x_8)
\end{cases}
\tag{35}
$$

where the inertia matrix I is modified by the mass (x_7) and the forces and moments with respect the body-frame (F_{x_b,y_b,z_b}, M_{x_b,y_b,z_b}) are functions of the input vector, which contains the manipulable variables that trigger the control systems.

$$
\begin{aligned}
I &= f(x_7) \\
F_{x_b,y_b,z_b} &= f(U) \\
M_{x_b,y_b,z_b} &= f(U)
\end{aligned}
\tag{36}
$$

5 Implementation

Once the model of the problem is accomplished, it is required to define the inputs and the manipulable variables that are responsible for the rocket control, by setting also its operational ranges.

In addition, through these definitions, the framework is developed in order to accomplish the simulations and the control study.

Despite the real-time control that the Falcon 9 uses, this project is focused in analysing the landing control by simulating its trajectory and, thus, the required deviations to adjust the system to the desired parameters.

5.1 Centre of mass

The centre of mass of the first stage, x_{cm}, is dependent of the mass, since it depends on the quantity of fuel ejected. Thus, considering that it is located at 16.62 m from the bottom, when the propellant tank is filled with the amount required for the recovery, and at 14.90 m, when the needed fuel is consumed, knowing the mass properties from tables 2 and 3, this parameter as a function of time is achieved by taking into account a linear consumption through the mass.

$$x_{cm} = 14.71446064 - \frac{43}{5145000}\, m \qquad m \,\epsilon\, [m_{st}, m_0] \tag{37}$$

where m_{st} is the dry mass of the stage and m_0 its initial mass with the remaining fuel to perform the landing. This estimation of the centre of mass would be modified from the initial whenever the reignition of the engines occurs.

Regarding to the centre of pressure, it is considered to be constant and situated at 14 m from the base, $x_{cp} = 14\,\text{m}$.

5.2 Moments of inertia

Given the symmetry of the structure and considering that the body-frame is within the principal axes of inertia, the remaining inertia tensor would be a diagonal matrix, since the non-diagonal terms can be neglected under these hypotheses. Moreover, by simplifying the stage geometry for a cylinder [27], these moments of inertia would be the following:

$$\begin{aligned} I_{xx} &= \tfrac{1}{2} m {R_{st}}^2 \\ I_{yy} = I_{zz} &= \tfrac{1}{12} m \left(3{R_{st}}^2 + \ell^2\right) \end{aligned} \tag{38}$$

where, as it can be noticed, these would depend on the instantaneous stage mass m, its radius R_{st} and length ℓ.

Nevertheless, these expressions are with respect to a centred frame and, consequently, they must be represented at its centre of mass within the body reference system using the Steiner's theorem.

$$\begin{aligned} I_{xx,cm} &= \tfrac{1}{2} m {R_{st}}^2 \\ I_{yy,cm} = I_{zz,cm} &= \tfrac{1}{12} m \left(3{R_{st}}^2 + \ell^2\right) - m \left(23.75 - x_{cm}\right)^2 \end{aligned} \tag{39}$$

5.3 Atmosphere

The atmosphere, as stated in section 4, is modelled with the standard atmosphere tables, but in the implementation, the COESA (Committee on Extension to the Standard Atmosphere) block from the Aerospace Blockset, an add-on of Simulink, will be used. It has a larger range of altitudes and the ones out of this can be extrapolated.

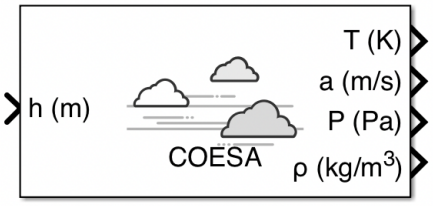

Figure 19: COESA atmosphere block

5.4 Inputs and variables

From the equation (35), the different state variables were defined and, aiming to characterise the problem, the tables below details the values and ranges in between the inputs and the variables are set, respectively. These parameters would be introduced into the framework by employing the Matlab code attached in the section B.1 of the annexes.

Table 3: Inputs summary [10] [11] [28]

Dimensions	
R_{st}	1.83 m
$d_{T_{N_2}}$	(42.00 - x_{cm}) m
r_{fin}	5.33 m
d_{fin}	(41.00 - x_{cm}) m
$\alpha_{\max}$	$\pm 90.00°$
$\delta_{\max}$	$\pm 25.00°$
S_{ref}	173.85 m^2
ℓ	47.50 m
Initial conditions	
m_0	228,000.00 kg
h_0	80,000.00 m
V_0	2,833.33 m/s
α_0	50.00°
$[\phi_0 \ \theta_0 \ \psi_0]$	$[0.00 \ \ 45.00 \ \ 0.00]$ °
$[p_0 \ \ q_0 \ \ r_0]$	$[0.00 \ \ -0.30 \ \ 0.00]$ °/s

Thrust parameters	
I_{sp}	282.00 s
Fins parameters	
t	1.50 m
c	7.00 m
$S_{ref,fin}$	21.00 m^2
$S_{wet,fins}$	25.00 m^2
np	66.00
$C_{N\alpha}$	0.067
$C_{N\delta,fin}$	0.020

Table 4: Control variables summary [10] [11]

Thrust	
T	0 – 2,562 kN
ε_z	0 – 10 °
ε_x	0 – 10 °
Cold gas thrusters	
T_{N_2}	0 – 1,500 N
ν_z	-90 – 90 °
ν_x	0 – 90 °
Grid fins	
δ	-25 – 25 °

5.5 Framework

The environment used in the implementation is Simulink from Matlab, which is based on blocks diagram. Thus, the general arrangement of the model system is attached bellow.

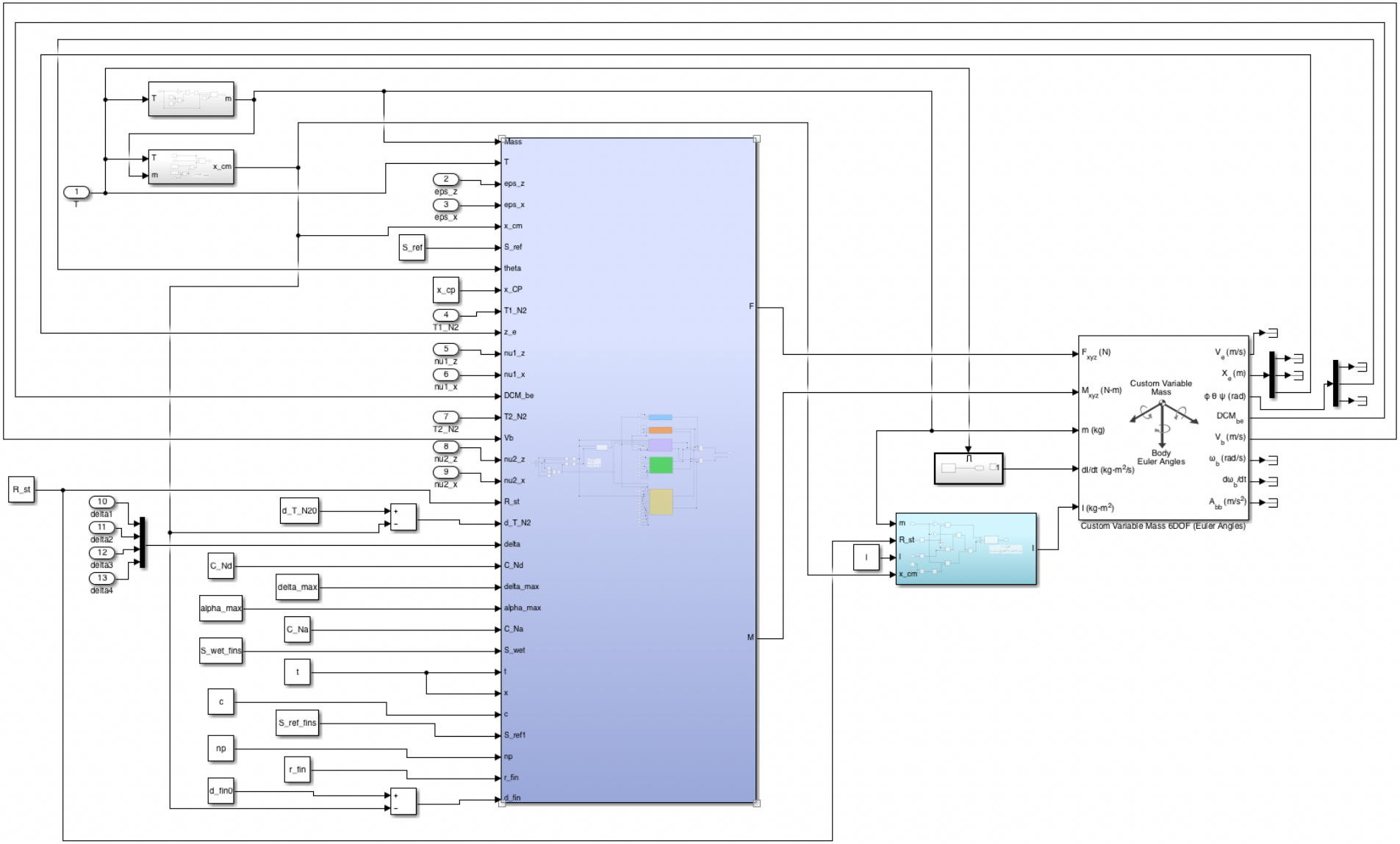

Figure 20: Simulink model

It can be seen that the overall diagram is formed with a blue block, which calculates the forces and the moments in body-axes, and they are introduced in a solver block. Moreover, the inputs of these system are the ones that are expected to control its performance.

Deepening in the block in which the forces and moments are calculated, it is divided in subsystems where the gravitational, thrust, aerodynamic, cold gas thrusters and grid fins forces are respectively computed through the model equations from 4, in order to obtain the resultant forces and meanwhile these are multiplied by its moment arm to obtain the global moments.

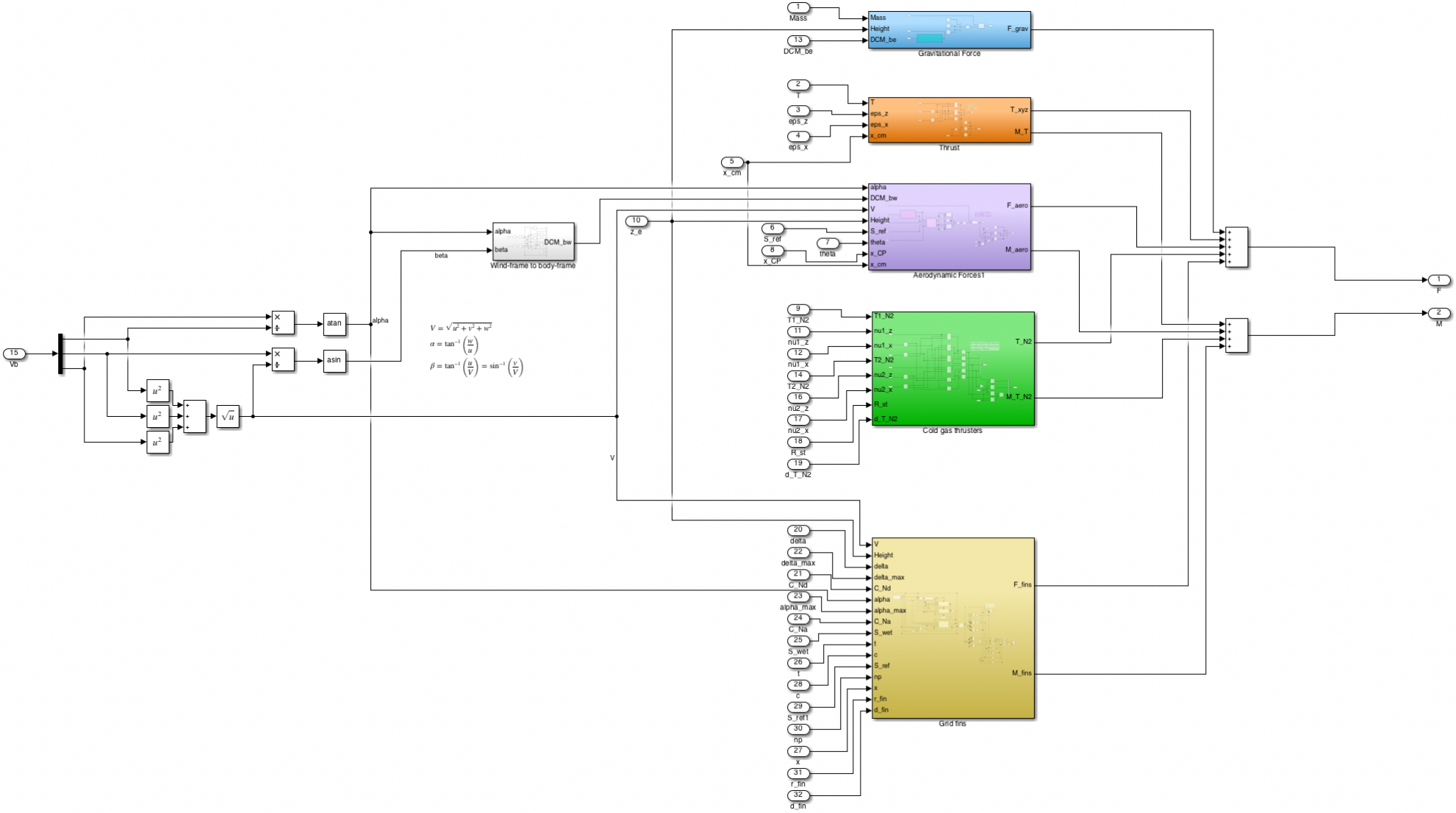

Figure 21: Forces and moments block subsystem

Afterwards, these parameters are needed in the following block which integrates and solves the 6-DOF (Degree Of Freedom) motion equations with a custom variable mass and through the Euler Angles. In particular, the block from Aerospace Blockset is employed:

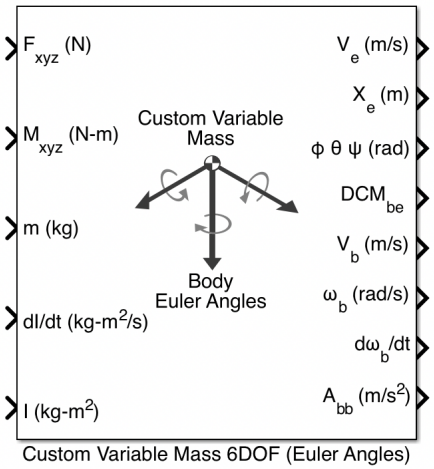

Figure 22: 6-DOF with custom variable mass and Euler Angles equations solver block

where, in addition to both the previous mentioned inputs, the current mass and inertia matrix, as well as the variation along time of this last parameter, are required. Moreover, the mass and inertia variation is within an enabled system, which is triggered whenever the engines are reignited, since it is when the loss of mass is involved.

Consequently, with these inputs and the initial conditions from table 3, the observable results of this block would be the velocity and position in Earth reference frame, the Euler angles, the rotation matrix from the Earth-frame to the body-frame, the linear and angular velocity in the body reference frame, the angular acceleration in body-fixed axes and the linear acceleration with respect to inertial frame, respectively in the figure order.

Furthermore, the height, the rotation matrix and the velocity in body-axes act as feedback to the preceding forces and moments block.

In order to deepen into this Simulink model, the overall system is attached in the section A.1 of the annexes.

5.6 Open loop model validation

With the aim of justifying the need of a control system and validate the results, the model is simulated without the control system. Hence, the next results can be achieved.

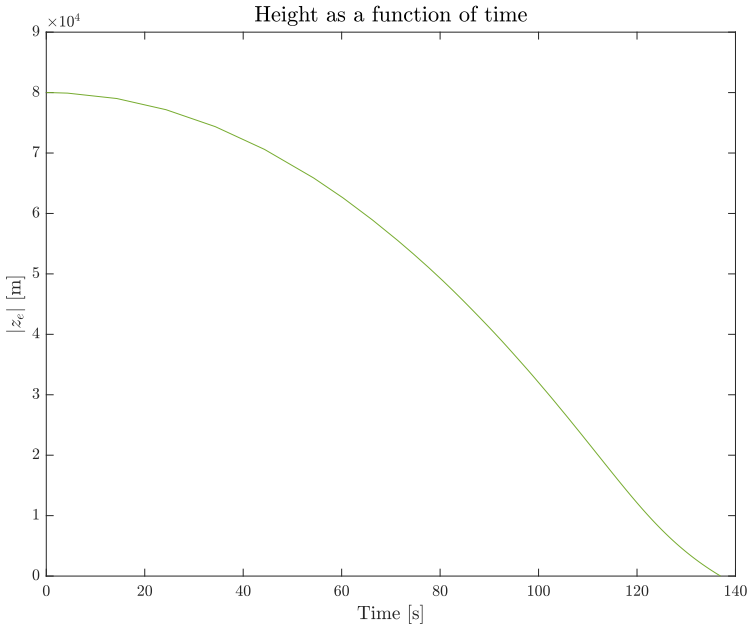

Figure 23: Height with respect to the inertial frame as a function of time

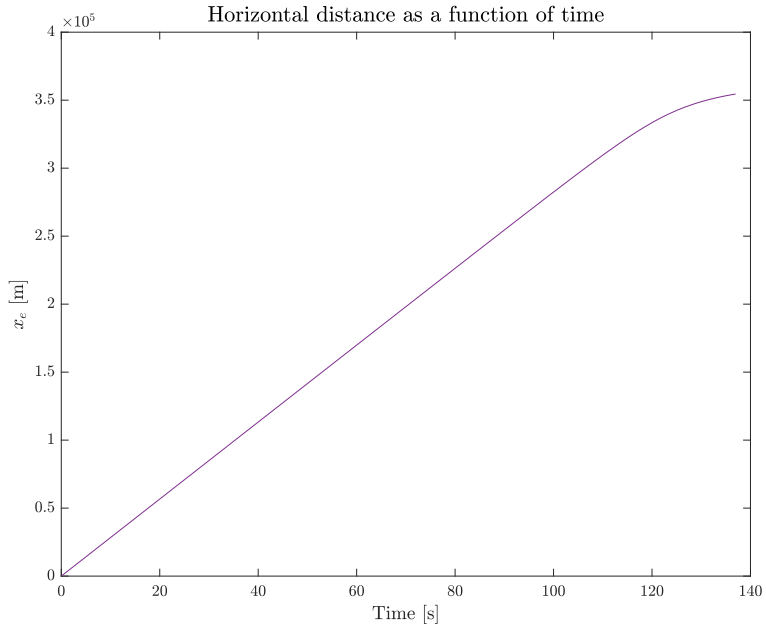

Figure 24: Horizontal distance with respect to the inertial frame as a function of time

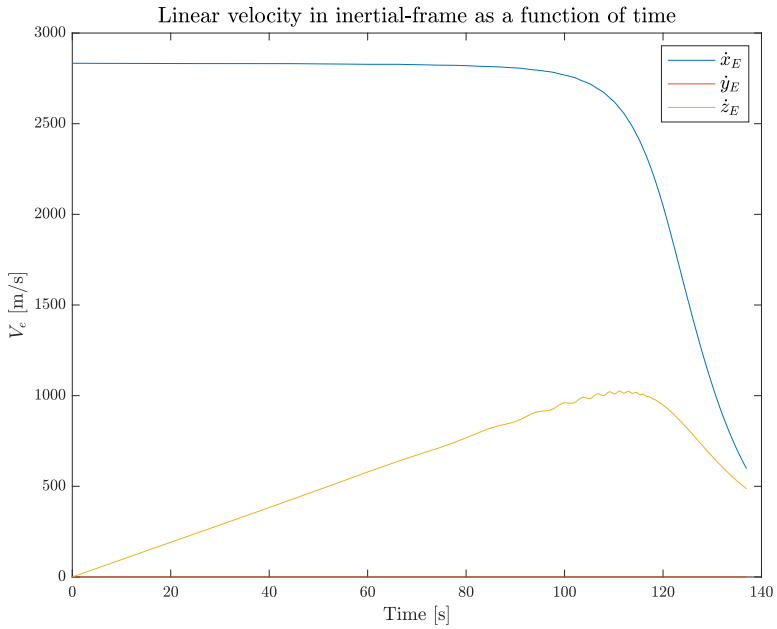

Figure 25: Linear velocity with respect to the inertial reference frame as a function of time

Considering that the remaining forces are just the gravitational and the aerodynamic, the graphs demonstrate compliance with the expected behaviour, a projectile motion. Nonetheless, the range is a bit larger because of the mass variation, which is considered to decrease linearly with the initial time, since the thrust is not taken into account in this case. Moreover, the movement perpendicular to the trajectory plane is null.

In addition, it is noticeable that the velocities at lower altitudes are drastically reduced, due to the increase of the aerodynamic forces, however, these are not sufficient to accomplish a safe landing and a vertical position of the stage is also required. This effect of the aerodynamic forces is given by the speed irregularities because of the uncontrolled stage rotation and, for a better understanding, it is represented the results omitting these forces.

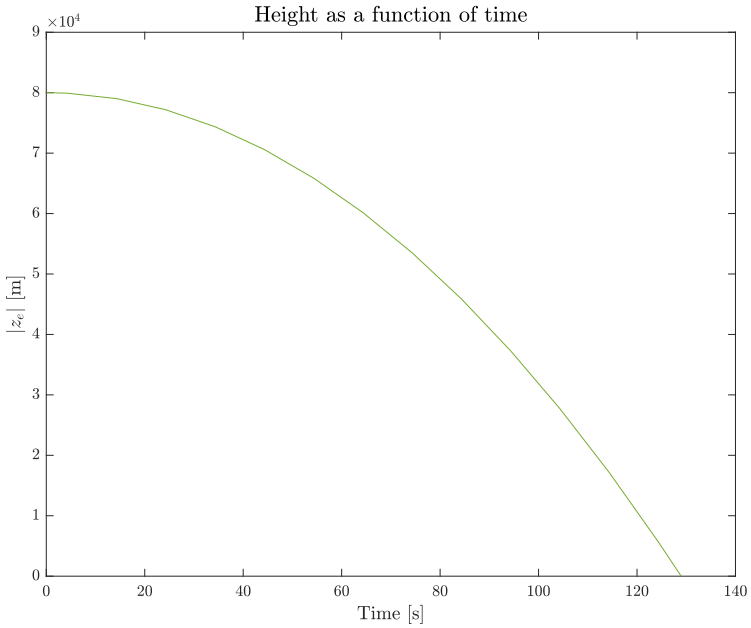

Figure 26: Height with respect to the inertial frame as a function of time neglecting the aerodynamic forces

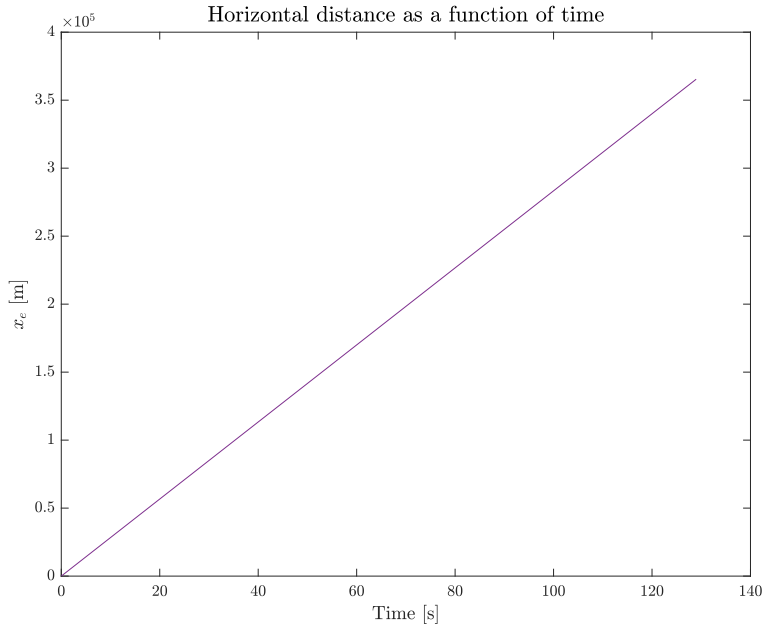

Figure 27: Horizontal distance with respect to the inertial frame as a function of time neglecting the aerodynamic forces

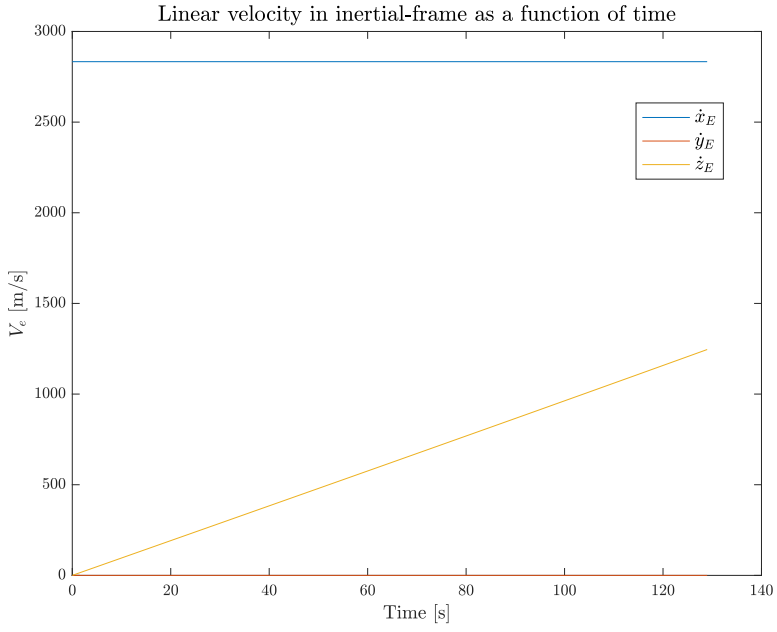

Figure 28: Linear velocity with respect to the inertial reference frame as a function of time neglecting the aerodynamic forces

It can be appreciated that, due to the lack of drag and lift forces, the horizontal velocity remains constant meanwhile the vertical component is increased with an almost constant slope, since the gravity variation is quite slight, from 9.58 m/s^2 to 9.81 m/s^2 approximately.

For these reasons and since the aerodynamic forces must be taken into account given its magnitudes, the lack of a control system has a clear visibility in the open loop model simulation and its relevance in the problem can be appreciated.

6 System control

Once the importance of controlling the system is appreciated, it is necessary to know the corresponding values that the control variables must reach in order to fulfil a safe landing.

Hence, different methodologies are studied with the aim of detecting results contrast and analysing the optimal behaviour.

6.1 Linearization

Firstly, most of the basic control systems require linearizing the equations in the interest of meeting the following model:

$$\begin{cases} \dot{\Delta x} = A\Delta x + B\Delta u \\ \Delta y = C\Delta x + D\Delta u \end{cases} \tag{40}$$

And from this state space representation, the transfer function, $G(s)$ [29], is achieved:

$$G(s) = \frac{Y(s)}{U(s)} = C(sI - A)^{-1}B + D \tag{41}$$

where A is the system matrix, B the input matrix, C the output matrix and D the feedthrough matrix.

Nevertheless, the importance of an adequate control for these complex systems mainly remains in selecting the points in which the equations are linearized around. As stated in several articles, such as [30], which study simple control methods for sophisticated systems, the selected points tend to be the mean values between the range in which the different state variables are comprised within its performance or just its desired final value. Hence, these will be studied in each particular case.

6.2 PID control

One of the first techniques to control the problem that will be studied is the PID control, a control loop feedback mechanism that consists in defining an error value as the difference between a desired setpoint and a measured process variable and applying a correction based on proportional, integral, and derivative terms of it.

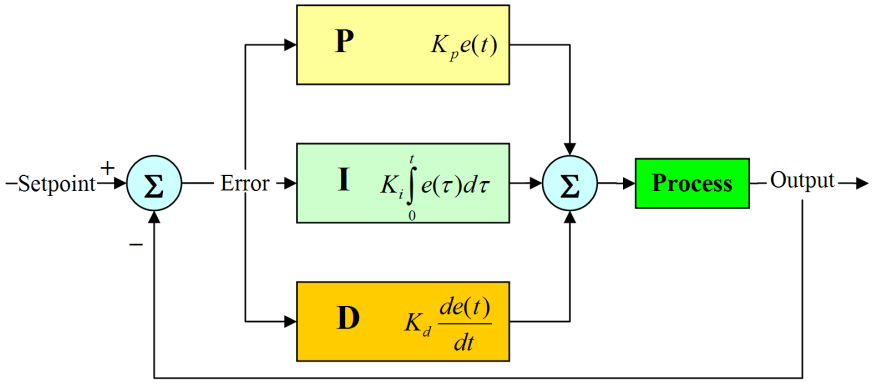

Figure 29: PID controller blocks diagram

6.2.1 Pitch control

Therefore, the first relevant parameter that needs to be controlled is the pitch angle of the stage, since as mentioned in section 3 there is an initial flip manoeuvre and the final angle must be $\theta = 90°$ in order to achieve a vertical landing.

Nonetheless, given the non-linear equations and its complexity, it is firstly simplified the system by just taking into account the gravitational and aerodynamic forces, focusing on this pitch control. This new model is described in the section A.2 of the annexes.

Moreover, the initial velocity is set to $V_0 = [2 \ 0 \ 1] \cdot 10^3$ m/s, since it demonstrates closer results to the expected ones. It is worth mention that it could not be employed within the previous open model, because, given the uncontrolled pitch, a singularity was obtained.

Consequently, after many iterations by testing the control taking as an input different variables, such as the linear body-frame velocity V_b or the angular body-frame velocity ω_b, the moments in the body y-axis are set as the optimal input, since the other cases has strong non-linearity and does not fit adequately to a given setpoint.

Hence, by linearizing the involved equations with the Model Linearizer App, an output named *linsys* is achieved and, through the Matlab code attached in the section B2 from the annex, the following transfer function is obtained:

$$G(s) = \frac{3.178{\cdot}10^{-8}s^3{+}1.168{\cdot}10^{-12}s^2{+}7.894{\cdot}10^{-13}s{-}1.455{\cdot}10^{-15}}{s^5{+}4.096{\cdot}10^{-7}s^4{+}1.501{\cdot}10^{-3}s^3{+}4.917{\cdot}10^{-6}s^2{-}1.591{\cdot}10^{-6}s{-}1.153{\cdot}10^{-8}} \tag{42}$$

It can be observed that it is a fifth order transfer function. On account of it, the below diagrams blocks is formed in order to calibrate the correspondent PID, with a step function as a setpoint.

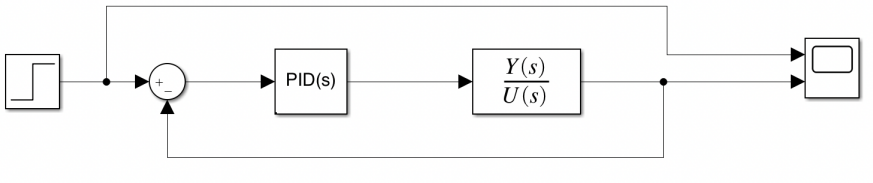

Figure 30: PID control blocks diagram through the transfer function

With the Simulink PID tuner, which finds the optimal constants by adjusting the time response and its robustness, the following values are accomplished:

$$k_p = 3.066 \cdot 10^6 \qquad k_i = 3.448 \cdot 10^4 \qquad k_d = 6.060 \cdot 10^7 \tag{43}$$

which, despite of being notably large numbers, it is justified with the considerable order of magnitude in which the moments are situated.

And the same sketch is pursued in the main simplified model, but changing its setpoint into the desired, which consists of an initial ramp from θ_0 up to 180°,

where it is maintained for a few seconds, and afterwards a negative ramp down to 90° that is the final desired value in which it is remained until the stage touchdown.

6.2.2 Controlled pitch results

It is worth mention that the setpoint has some restrains, as stated in the section A.2 from the annexes, given the rank of pitch angles that the solver block admits is between –180° to 180°, thus, since the controller has some overshooting, this setpoint must be slightly smaller in order not to excess this values nor obtain singularities.

Besides that, it would result in the following controlled output.

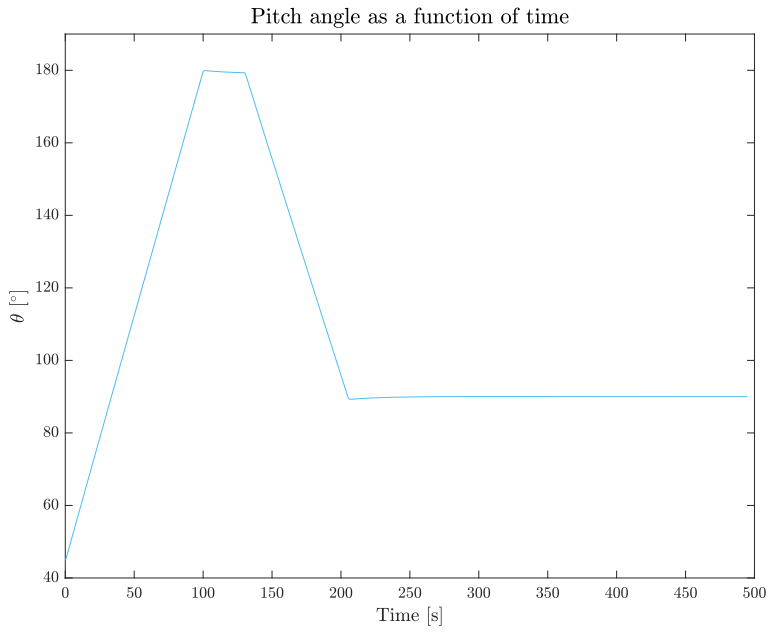

Figure 31: PID controlled pitch as a function of time

As it can be seen it adapts excellently to the desired performance, robustly and with the lack of relevant overshoots.

6.2.3 Velocity control

Nonetheless, by only controlling the pitch is not enough to fulfil a soft landing, since at the touchdown the stage would possess too much velocity. Thus, a velocity module inferior to 2 m/s is considered to be an adequate speed to complete a safe landing.

Likewise the procedure employed previously, through iterating with different variables to control this final value of the linear velocity module, the most effective parameter to control is the forces. Since the equations can be simplified by considering that the forces are detached from each axis, as stated in [14], they will be studied separately.

Despite having to adapt each control individually, the methodology pursued for each one of the forces is equivalent. A new subsystem is introduced in order to calculate the needed resultant forces required to reach the desired velocity profile in each component, which basically decelerate the stage until a safe landing speed. This block would be the analogous to the overall forces that the main thruster engines should contribute to accomplish the setpoint.

Hence, the control is achieved with a negative feedback of the gravitational and aerodynamic forces and a simple proportional control with k_p= 1, since it is needed to set the forces to its requested value in order to obtained the expected controlled output, which is the velocity in its corespondent axis.

In spite of the difficult automation of this process, due to the need of adjustments of the setpoint as a function of the inputs, it is the most effective linear control to perform this landing.

6.2.4 Controlled velocity results

Consequently, applying this control, added to the pitch control, the results are displayed below.

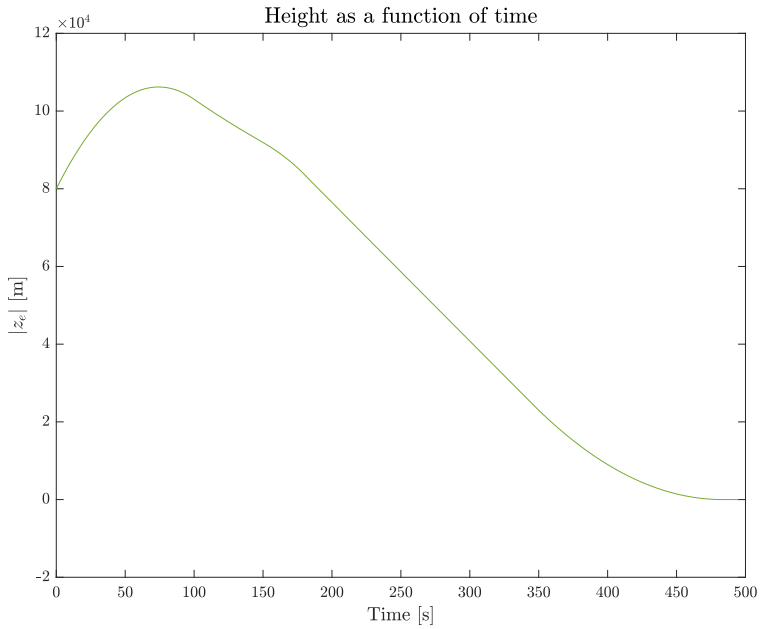

Figure 32: Height with respect to the inertial frame as a function of time by a PID controller

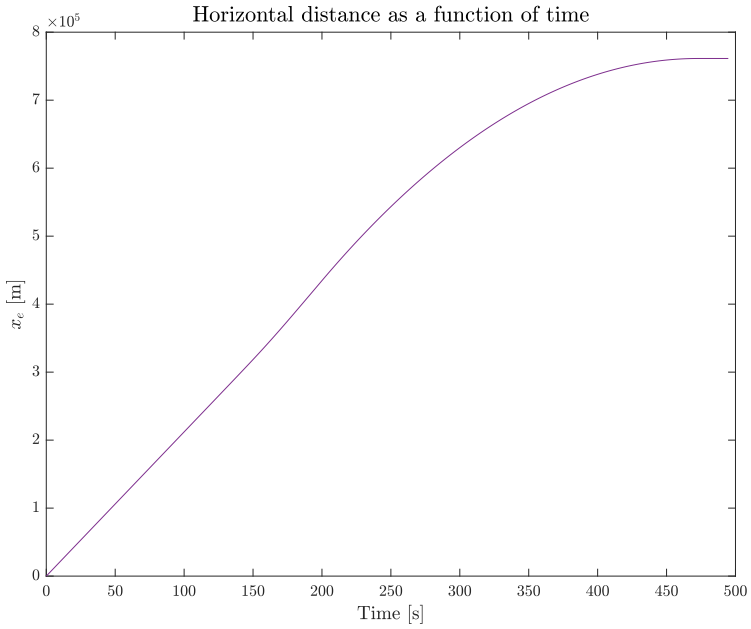

Figure 33: Horizontal distance with respect to the inertial frame as a function of time by a PID controller

It can be observed that the height has similar behaviour to the expected, as it can be noted in the sketch from figure 11, and along with the horizontal distance they have a tendency to maintain its value at the final phase, since the velocity is drastically diminished.

Regarding this last parameter, its profile can be studied with its module.

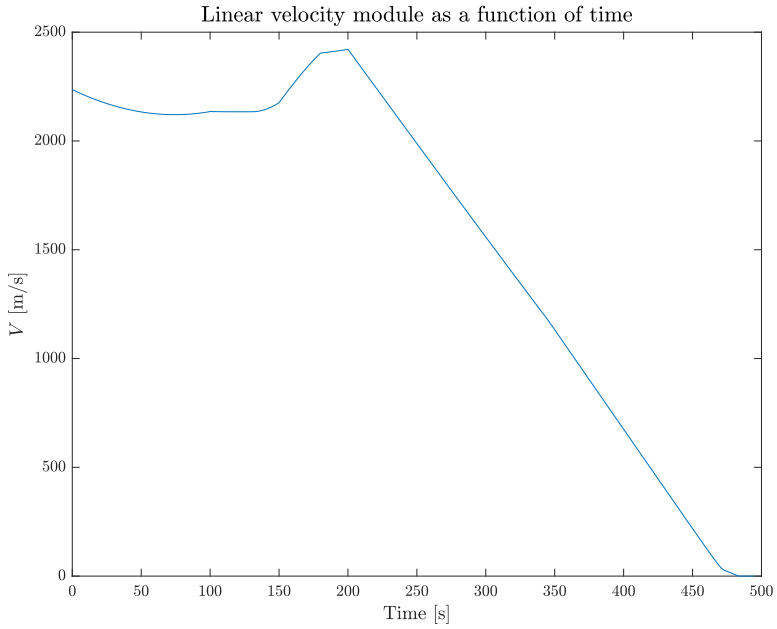

Figure 34: Velocity module with respect to the inertial frame as a function of time by a PID controller

In the figure, the initial diminution of the speed is appreciated, due to the gravity effect on its initial upwards velocity that would add a negative component to it, and afterwards an increase because of the gravity turn manoeuvre, which, given the effect of the controlled forces, its velocity would be further decreased until the final value of 0.09 m/s approximately, being remarkably inside its safe range.

Finally, with the aim of witnessing these results in a more pragmatical way, the trajectory of the stage is plotted.

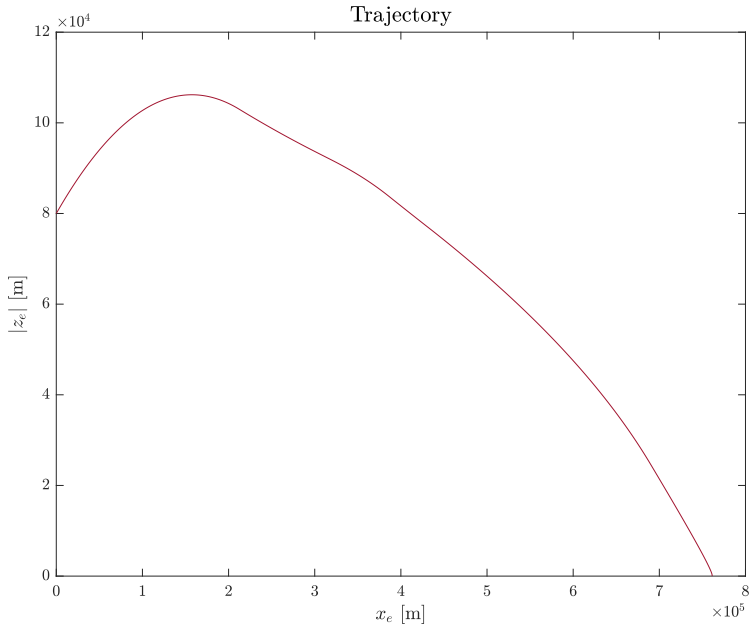

Figure 35: Trajectory with respect to the inertial frame by a PID controller

In definitive, the obtained results fits completely to the desired parameters to perform a safe landing of the first stage of the Falcon 9. Nevertheless, since it has been just verified with ideal conditions, without wind nor perturbations, the robustness of the control system has to be studied.

6.2.5 Perturbed system

Since the PID control to verify is mainly the pitch angle controller, the system is perturbed by adding constant values of moments to the ones from the controller output in order to simulate the wind conditions. It could be analysed through the forces, however, given that the controller output are moments, they would possess a less relevant impact to the system.

Hence, with an order of moments of 10^4 N m in each axis, it will be required to set to 0 the moments in the body x and z axis, since it is only desired from the stage to perform within the pitch angle, in other words, to maintain the plane of the trajectory within the x-z plane. Consequently, by canceling the effects of

the perturbation with a simple negative feedback, the effectiveness of the PID controller for the body y-axis moments can be studied. Superposing, both the previous pitch angle result from figure 31 and the one from this new perturbed system it is achieved the diagram below.

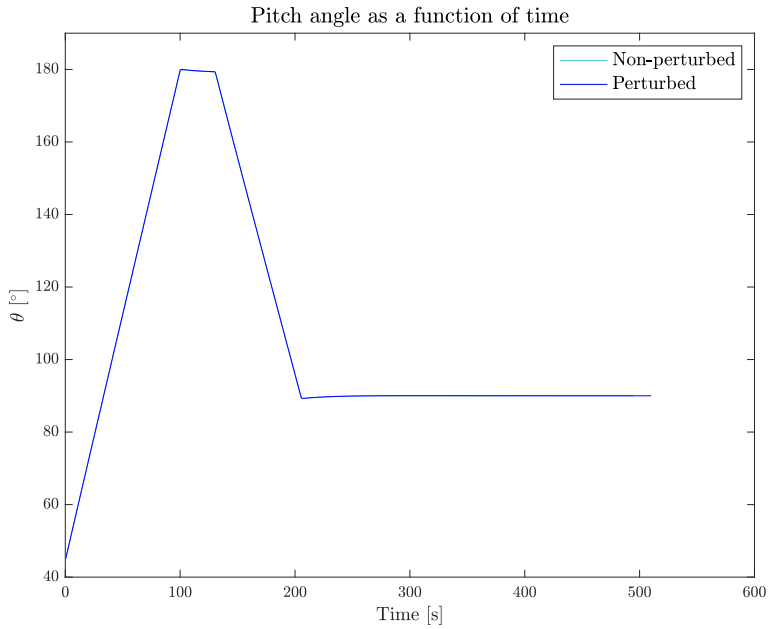

Figure 36: Pitch angle comparison between the non-perturbed and perturbed system by a PID controller

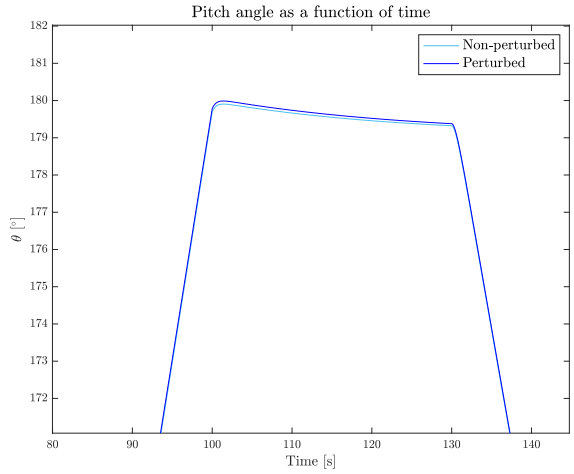

Figure 37: Zoomed pitch angle comparison between the non-perturbed and perturbed system by a PID controller

As it can be seen, the system acts as a robust control due to the similarity of the perturbed system with respect the ideal one. Moreover, with Matlab code of section B.3 from the annexes where the plots are represented, the maximum angle difference between these two simulations is also displayed, giving a small value of 0.148°.

Despite higher magnitudes of perturbation offers not desired results because of the slight overshooting in the horizontal flip, giving a value larger than 180° that entail a singularity to the solver block, since as aforementioned its valid rank is within –180° to 180°, it can be corrected by increasing the robustness of the controller. However, since the order of magnitudes from the wind and other perturbations remains just within this studied rank, it can be determined that the PID possesses the adequate control parameters.

Thus, it can be concluded that the pursued process offers the expected results, which adequately fulfil the aim of the project.

6.3 Model Predictive Control

With the purpose of comparing the pitch obtained results with another methodology, the Model Predictive Control (MPC) is also studied, which consists in a controller that minimises the error between the system response and the setpoint of the current time slot while keeping the future ones in account.

In the figure below, the performance of this controller is sketched, where important parameters of this controller appear. Firstly, the sample of time, which are the time divisions (horizontal axis), the prediction horizon, which is the number of future control intervals that the controller must evaluate by prediction when optimising at an interval k, and the control horizon, which is the number of future control intervals of the inputs of the system that are used to consider the prediction.

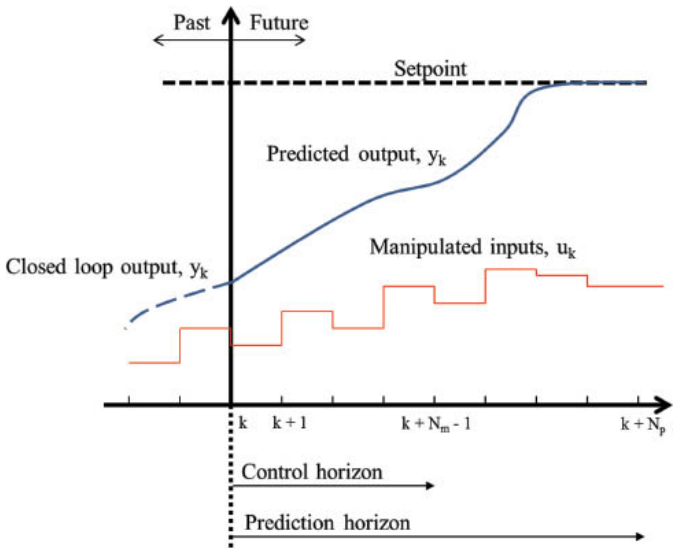

Figure 38: MPC performance diagram [31]

6.3.1 Pitch control

Once the bases of the controller are set, it is implemented in the framework by employing the Model Predictive Control Toolbox. Through this Matlab add-on, in the Simulink model, the MPC block can be applied.

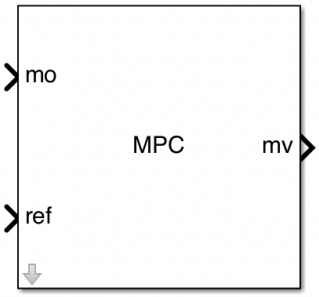

Figure 39: MPC Simulink block

This block controls the desired output (mo) with respect the introduced set-point (ref) and obtaining the corresponding control value (mv) with the explained methodology. In this case, they would be the pitch angle, its setpoint and the moments in the body y-axis, respectively in the previous order.

In order to configure this controller, the MPC Designer from the aforementioned Matlab toolbox is used, which linearizes the plant, takes into account the scale factors between the output and the input and offers the possibility of adjusting the controller parameters to obatin either a faster, a robuster or a more aggressive response. Thus, the response that best fits a given setpoint, by considering a sample time of 0.1 s, is an MPC with a prediction horizon of 5 and a control horizon of 2.

6.3.2 Controlled pitch results

Hence, following the diagram detailed in the section A.2 from the annexes, which controls likewise the previous PID control but modifying the controller. Consequently, the controlled pitch through the moments in the body y-axis and the MPC would present the performance displayed in the figure below.

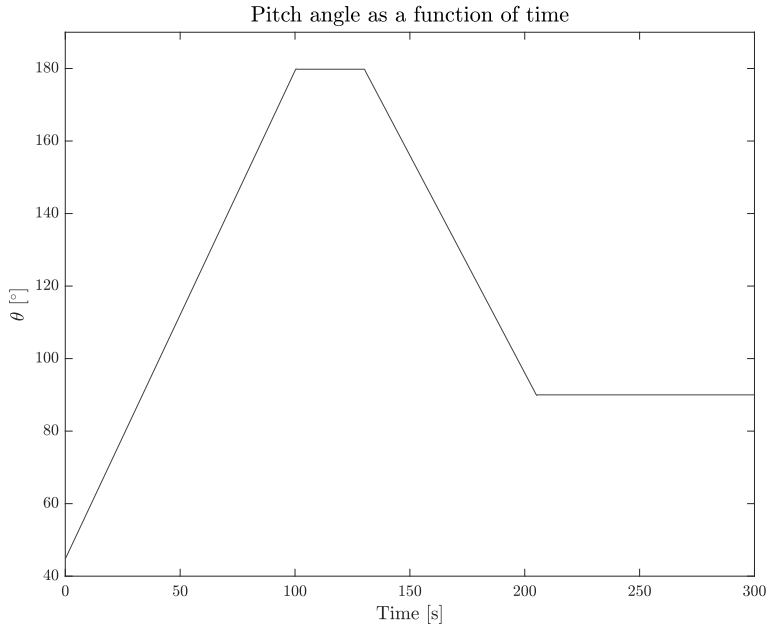

Figure 40: MPC controlled pitch as a function of time

It can be appreciated that the response to the setpoint is certainly fast with not significant overshooting in the overall performance. In addition, the setpoint

can be adjusted to values more proximate to the limit values (180°), since its overshooting is lesser than the resulted in the PID control.

For these reasons, the result demonstrates the adequacy of this control method, which also accomplishes the main objective of the project.

6.3.3 Perturbed system

Along the lines of the PID controller, it is relevant to verify the MPC behaviour by introducing perturbations into the system. Thus, analogous to the previous method, the controlled moments would be summed up to constant values with an order of 10^4 N m and the following comparison can be effectuated.

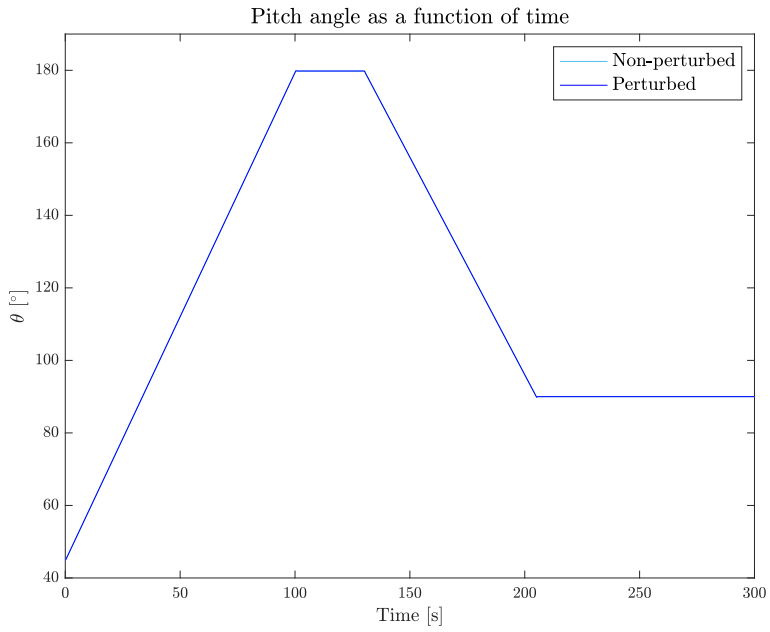

Figure 41: Pitch angle comparison between the non-perturbed and perturbed system by a MPC controller

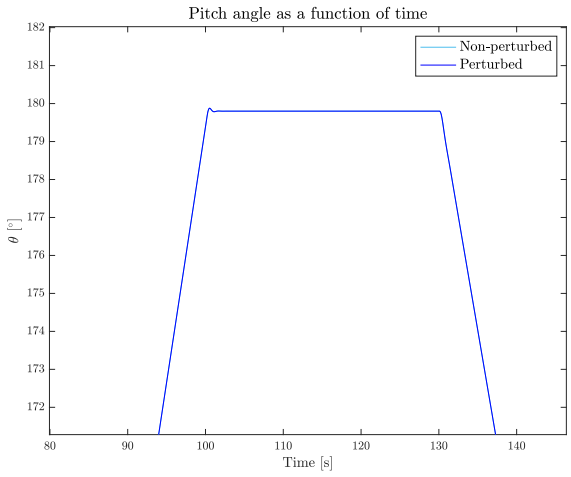

Figure 42: Zoomed pitch angle comparison between the non-perturbed and perturbed system by a MPC controller

It can be seen that the perturbations almost do not change the response behaviour, presenting a maximum angle difference of 0.003°. Moreover, in this case, the controller admits values with higher orders of moments in the perturbation, but, as stated in previous subsections, generally it would not be exceeded.

In addition, the MPC block permits to add as an input the disturbances of the system with the purpose of adapting the controller along it. The new entry is the one named as md in the following figure.

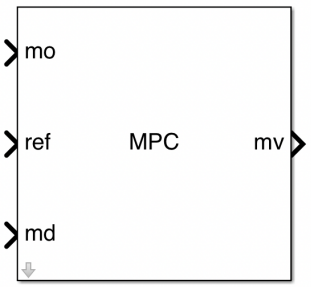

Figure 43: MPC Simulink block with disturbances

Nonetheless, this methodology is specially implemented in more complex disturbances and, since the already achieved result has a very small error, it can

determined that the designed MPC is an adequate controller for the system of the project.

6.4 Controllers comparison

Once the pitch is controlled with two different methodologies, they can be compared in order to select which is the most suitable for the system. As earlier mentioned, the MPC involves a faster and robuster response rather than the PID controller. For this reason, the presence of less overshooting in the MPC controlled system permits a more exact approach, since the setpoint is able to set closer to 180° without outstripping the solver block limitations.

The main distinctions of both controllers remain in the capacity of the MPC to anticipate future responses and take control actions accordingly, as opposed to PID controllers, which lack of this predictive ability.

Besides that, in order to perceive the stated differences, both achieved responses can be overlapped to compare them.

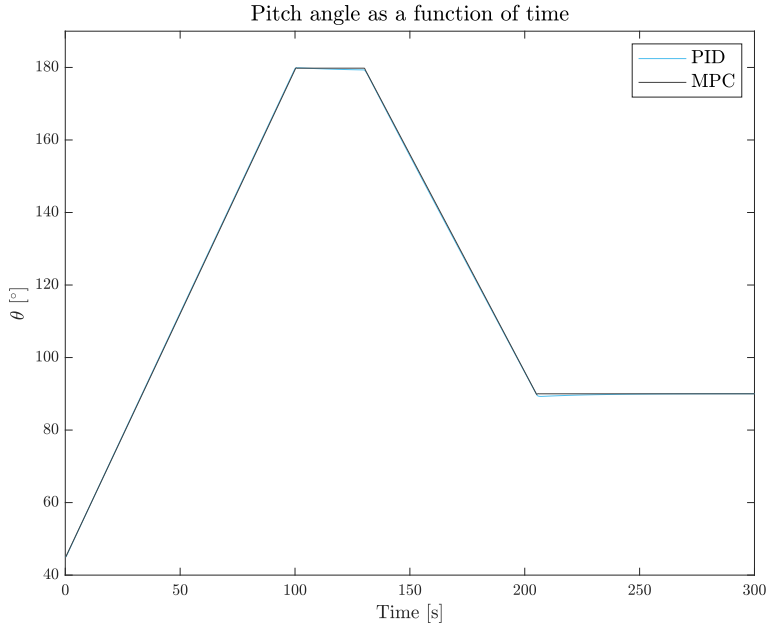

Figure 44: PID and MPC controlled pitch angle comparison

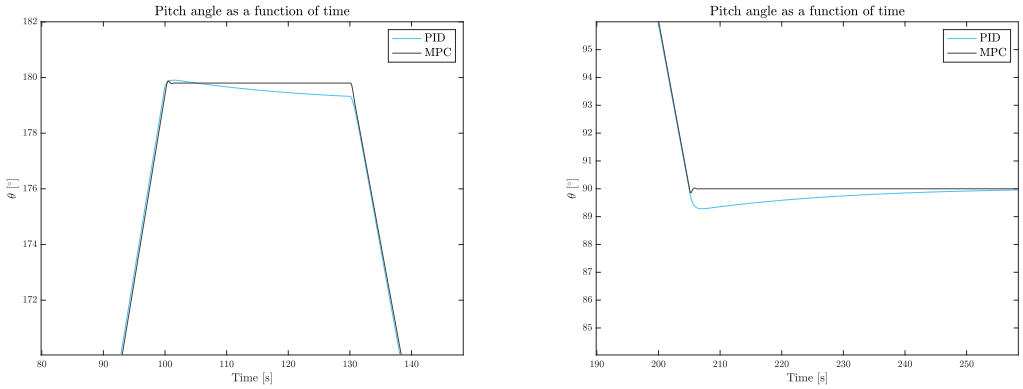

Figure 45: PID and MPC zoomed controlled pitch angle comparison

It can be appreciated that the result with the PID controller dispose of more overshooting, in particular in the changes between the ramp function into a constant value. Meanwhile, the MPC controlled response is faster and robuster, which remarkably sets into the introduced setpoint with an associated low error.

Furthermore, through the Matlab code attached in the section B.3 from the annexes, this error between the setpoint and the actual output is computed, achieving a mean value of 0.106° for the PID control and 0.078° for the MPC, and maximums of 0.716° and 0.412°, respectively.

In conclusion, the MPC controller offers a better performance rather than the PID, accomplishing a quicker response, which fits more suitable the introduced setpoint.

7 Budget summary

In this section, the summary of the budget, whose complete details are attached in the corresponding separated document, is displayed below.

The total cost to develop the project is 6,955.64 €, where the engineering hours, as well as the costs associated to the software, the equipment and the energy, are considered.

Table 5: Budget summary

Concept	Cost (€)
Engineering hours	6,825.00
Software	94.83
Equimpent	32.76
Energy	3.05

Total	6,955.64 €

8 Environmental impact

In this section, the environmental impact on the account of the elaboration of the thesis is studied.

The development of this project has been carried out during the pandemic situation of the Covid-19 and, for this reason, the consumption of transport to the university is not contemplated.

Nevertheless, the carbon footprint of the electricity consumed by the laptop is accounted and estimated to possess an impact factor of 0.22 kg CO_2/kWh, the the mean value from Spain [32]. Moreover, its power consumption of 61 W and the time duration of the project, 455 hours, are also taken into consideration. Thus, a total of 6.11 kg CO_2 is produced.

Regarding the environmental effect of the project results, the reusability of rockets diminishes some of the carbon footprint due to the decrease of the required consumption, since the effort of reconditioning their launch systems is certainly reduced [33], as well as the creation of new ones. Hence, the search for optimal controllers is relevant to contribute to the promotion of a more sustainable space launcher sector and this is the reason why Europe is taking the first steps towards the development of reusable rockets [34].

9 Conclusions

Through this project, the control for the launch system of a rocket has been studied, centring it into the implementation of the first stage recovery from the Falcon 9 of the SpaceX.

Firstly, the analysis of the 6 degrees of freedom equations particularised for the problem is effectuated, in order to introduce them into the framework developed within the Matlab and Simulink environment. This program imports the inputs from a Matlab script and solves the problem through the blocks diagram created with Simulink.

Once the first simulations are represented, the need of a control system is noticeable, since the parameters of a safe landing are not accomplished, being the most important the final velocity at the touchdown. Hence, different linear controllers are applied to the system. Nevertheless, given the non-linearity and the complexity of the problem, which dispose of several control inputs, it is simplified computing the resultant forces and moments from the overall control devices. This model offers a linearly controllable performance, since its linearized system fits better rather than the previous one.

Consequently, following the Falcon 9 landing, the pitch is controlled to carry out an horizontal flip and a final vertical landing. A suitable method to control it is through the moments, thus PID and MPC controllers are analysed, obtaining for both adequate results, certainly similar to its desired setpoint and with a robust reaction among external perturbations, in other words, these controllers are able to adapt to any wind conditions or other perturbations. Nonetheless, the MPC entails a faster response and with a slightly less overshooting associated. For this reason, this controller can be considered the optimal for the studied case.

Regarding the soft landing condition, the control could not be reached likewise

the methodology employed for the pitch, given the limitations of its nonlinear equations. Instead, it is developed by setting the required forces to achieve the desired profile of velocities, obtaining a final speed considerably close to 0 m/s.

In conclusion, the first stage recovery of the Falcon 9 is a complex problem, which has finally been approached to a controlled system. The pitch offers a remarkable response with a MPC controller for the moments and the forces can be correspondingly established to accomplish the desired velocities. Besides that, more advanced control techniques, such as non-linear controllers, are required to seek a more automatic control for the velocities or to compute each control device separately, which can be studied for further projects.

9.1 Future work

This thesis implements a first approach to the recovery control of launch systems of rockets and, despite the principal aim of the project has been accomplished, there are improvements that could be further applied.

Firstly, the aerodynamic models of the structure and the real atmosphere could be incorporated into the framework, which could be easily substituted for the corresponding current blocks. Thus, the simulations would be more similar to the real time performance.

Furthermore, the speed could be controlled with more advanced methods, such as the Feedback Local Optimality Principle [35] or the sliding mode control [36], which are nonlinear controllers. Moreover, the successive linearization approach could also be studied [37], yielding a linear and time-varying description of the system that increase the control capacity through linear controllers.

Finally, with the purpose of taking into account the control devices individually, along the lines of the previous proposals, these techniques could also be

effective to implement a second layer of control, where the different inputs from each control surface would be calculated from the respective already computed forces and moments that the overall must adopt in order to control the pitch and the velocity. Hence, the main engines thrust could be responsible for the forces control and the cold gas thrusters and the grid fins for the moments, considering also their respective contributions.

References

[1] Robert Tománek and Jakub Hospodka. "Reusable Launch Space Systems". In: *MAD - Magazine of Aviation Development* 6 (May 2018), pp. 10–13. DOI: 10.14311/MAD.2018.02.02.

[2] Lars Blackmore. "Autonomous precision landing of space rockets". In: 46 (Jan. 2016), pp. 15–20.

[3] Jackie Wattles. "Why Crew Dragon will land in water". In: *CNN Business* (Aug. 2020). URL: https://edition.cnn.com/business/live-news/nasa-spacex-mission/h_c1ca82bb0c906b3021624ac05faae25c.

[4] *Rocket Lab*. URL: https://www.rocketlabusa.com/ (visited on 03/03/2021).

[5] *NASA*. URL: https://www.nasa.gov/ (visited on 02/23/2021).

[6] Emily Calandrelli. "Blue Origin Launches and Lands Recovered Rocket". In: *TechCrunch* (2016). URL: https://techcrunch.com/2016/01/23/blue-origin-launches-and-lands-recovered-rocket/?guccounter=1.

[7] *SpaceX*. URL: https://www.spacex.com/ (visited on 02/23/2021).

[8] *Fairing Recovery Attempts*. Mar. 2020. URL: https://www.elonx.net/fairing-recovery-attempts/ (visited on 02/23/2021).

[9] *Blue Origin*. URL: https://www.blueorigin.com/ (visited on 03/03/2021).

[10] SpaceX. *Falcon User's Guide*. Tech. rep. 2020. URL: https://www.spacex.com/.

[11] Ed Kyle. *SpaceX Falcon 9 v1.2 Data Sheet*. Mar. 2021. URL: https://www.spacelaunchreport.com/falcon9ft.html (visited on 03/07/2021).

[12] Michael Howard, Michael Deep, and Scott Schilke. "GALLERY: SpaceX launches Bangabandhu-1 atop Block 5 Falcon 9". In: *SpaceFlight Insider* (May 2018). URL: https://www.spaceflightinsider.com/photo-galleries/gallery-spacex-launches-bangabandhu-1-atop-block-5-falcon-9/nggallery/page/1.

[13] Miguel Ángel Gómez Tierno, Manuel Pérez Cortés, and César Puentes Márquez. *Mecánica del Vuelo*. 2nd. Garceta Grupo Editorial, 2012, pp. 1–44. ISBN: 9788415452010.

[14] Aliyu Bhar Kisabo and Aliyu Funmilayo Adebimpe. "State-Space Modeling of a Rocket for Optimal Control System Design". In: *Journal of Aircraft and Spacecraft Technology* May (2019). DOI: 10.5772/intechopen.82292.

[15] Q. Zong, F. Wang, and B. L. Tian. "Nonlinear adaptive filter backstepping flight control for reentry vehicle with input constraint and external disturbances". In: *Proceedings of the Institution of Mechanical Engineers, Part G: Journal of Aerospace Engineering* 228.6 (2013), pp. 889–907. ISSN: 20413025. DOI: 10.1177/0954410013482238.

[16] P Bollino Kevin. *High-fidelity real-time trajectory optimization for reusable launch vehicles*. 2006. URL: https://calhoun.nps.edu/handle/10945/10056.

[17] Xinfu Liu. "Fuel-optimal rocket landing with aerodynamic controls". In: *Journal of Guidance, Control, and Dynamics* 42.1 (2019), pp. 65–77. ISSN: 15333884. DOI: 10.2514/1.G003537.

[18] Frank J. Regan and Satya M. Anandakrishnan. *Dynamics of Atmospheric Re-Entry*. American Institute of Aeronautics and Astronautics, Jan. 1993. DOI: 10.2514/4.861741.

[19] Bailing Tian and Qun Zong. "Optimal guidance for reentry vehicles based on indirect Legendre pseudospectral method". In: *Acta Astronautica* 68.7-8

(Apr. 2011), pp. 1176–1184. ISSN: 00945765. DOI: 10.1016/j.actaastro.2010.10.010.

[20] University of North Texas Libraries. *Standard Atmosphere - Tables and Data for Altitudes to 65,800 Feet*. Tech. rep. UNT Digital Library, 1955. URL: https://digital.library.unt.edu/ark:/67531/metadc65571/m1/16/.

[21] Timothy W. Ledlow, John E. Burkhalter, and Roy J. Hartfield. "Integration of grid fins for the optimal design of missile systems". In: *AIAA Atmospheric Flight Mechanics Conference, 2015*. American Institute of Aeronautics and Astronautics Inc., 2015. ISBN: 9781624101328. DOI: 10.2514/6.2015-1017.

[22] HyeongJin Lee et al. "Aerodynamic Characteristics of the Grid Fins on SpaceX Falcon 9". In: *Korean Society for Aeronautical and Space Sciences* 48.10 (2020), pp. 745–752. DOI: 10.5139/JKSAS.2020.48.10.745. URL: https://doi.org/10.5139/JKSAS.2020.48.10.745.

[23] G. A. Faza et al. "Study of Swept Angle Effects on Grid Fins Aerodynamics Performance". In: *Journal of Physics: Conference Series*. Vol. 1005. 1. Institute of Physics Publishing, May 2018. DOI: 10.1088/1742-6596/1005/1/012013. URL: https://iopscience.iop.org/article/10.1088/1742-6596/1005/1/012013.

[24] P. Theerthamalai. "Aerodynamic Characterization of Grid Fins at Subsonic Speeds". In: *Journal of Aircraft* 44.2 (Mar. 2007), pp. 694–698. ISSN: 0021-8669. DOI: 10.2514/1.27653.

[25] NASA. *Air Viscosity*. URL: https://www.grc.nasa.gov/WWW/k-12/airplane/viscosity.html (visited on 04/20/2021).

[26] Allard Overmeen. "What is the difference between laminar flow and turbulent flow?" In: *Bronkhorst* (Mar. 2020). URL: https://www.bronkhorst.com/int/blog-1/what-is-the-difference-between-laminar-flow-and-turbulent-flow/.

[27] Raymond A Serway. *Physics for scientists & engineers*. 2nd. Philadelphia: Saunders College Pub., 1986, p. 202. ISBN: 0-03-004534-7.

[28] Office of Safety and Mission Assurance (OSMA). *Space Launch Report: SpaceX Falcon 9 v1.1 Data Sheet*. Tech. rep.

[29] Fatiha Nejjari and Joseba Quevedo. *Tema 2. Modelització de sistemes dinàmics*. Tech. rep. 2019.

[30] James C. Hung and Joel David Hewlett. "PID control". In: *Control and Mechatronics*. 2016. Chap. 11. ISBN: 9781439802885. DOI: 10.3156/jfuzzy.7.4_768.

[31] Shannon Ewanick et al. "Use of Raman spectroscopy for continuous monitoring and control of lignocellulosic biorefinery processes". In: *Pure and Applied Chemistry*. Vol. 86. 5. IUPAC Secretariat, May 2014, pp. 867–879. DOI: 10.1515/pac-2013-1022. URL: https://www.degruyter.com/document/doi/10.1515/pac-2013-1022/html.

[32] *Carbon Footprinting*. URL: https://www.carbonfootprint.com/ (visited on 06/14/2021).

[33] Andres Torres. *Reusable Rockets and the Environment*. Tech. rep. Merced: University of California, May 2020.

[34] European Space Agency. "ESA plans demonstration of a reusable rocket stage". In: (2020). URL: http://www.esa.int/Enabling_Support/Space_Engineering_Technology/ESA_plans_demonstration_of_a_reusable_rocket_stage.

[35] Antonelli Dario et al. "Feedback Local Optimality Principle Applied to Rocket Vertical Landing (VTVL)". In: *Nonlinear Dynamics and Control* II (2020). DOI: 10.1007/978-3-030-34747-5.

[36] Liang Zhang et al. "Fixed-time extended state observer based non-singular fast terminal sliding mode control for a VTVL reusable launch vehicle". In: *Aerospace Science and Technology* 82-83 (Nov. 2018), pp. 70–79. ISSN: 12709638. DOI: 10.1016/j.ast.2018.08.028.

[37] Ashish Tewari. "Optimal Guidance of Rockets". In: *Advanced Control of Aircraft, Spacecraft and Rockets*. John Wiley & Sons, 2011. Chap. 4, pp. 195–296. ISBN: 9780470745632.